

Lincoln University Digital Thesis

Copyright Statement

The digital copy of this thesis is protected by the Copyright Act 1994 (New Zealand).

This thesis may be consulted by you, provided you comply with the provisions of the Act and the following conditions of use:

- you will use the copy only for the purposes of research or private study
- you will recognise the author's right to be identified as the author of the thesis and due acknowledgement will be made to the author where appropriate
- you will obtain the author's permission before publishing any material from the thesis.

**Spinal cord pathology of ovine CLN5 and CLN6
neuronal ceroid lipofuscinoses
(Batten disease)**

A thesis
submitted in partial fulfilment
of the requirements for the
Degree of Master
at
Lincoln University

by
Jazmine Lee Brash

Lincoln University
2023

Abstract of a thesis submitted in partial fulfilment of the requirements for the Degree of Master at Lincoln University

**Spinal cord pathology of ovine CLN5 and CLN6
neuronal ceroid lipofuscinoses
(Batten disease)**

by

Jazmine Lee Brash

Neuronal ceroid lipofuscinosis (NCL or Batten disease) is a fatal neurodegenerative disorder, which occurs in approximately 1 in 12,500 children worldwide and currently has no cure. To date, there are thirteen known variants of NCL, caused by mutations in the genes *CLN1-8* or *CLN10-14*. Two naturally occurring forms of CLN5 and CLN6 NCL exist in Borderdale and South Hampshire sheep breeds respectively. These large animal models recapitulate the clinicopathological features of the human disease and have been instrumental in understanding the human condition and in the development of gene therapies.

Affected sheep have a well-characterised pathogenic cascade in the brain, which begins prenatally and involves neurodegeneration, neuroinflammation and lysosomal storage, but very little is known about their spinal cord pathology. This study examined anatomy and neurochemistry in the healthy sheep spinal cord and then compared that to pathology in the CLN5 and CLN6 affected spine over the disease course. Neurodegeneration was assessed by area measurements and neuron counts. This revealed that there was no grey matter loss in the spinal cord for either diseased genotype, but total cross-sectional area and white matter spinal cord areas declined rapidly at end-stage disease (18 months of age). There was also an equivalent late-stage reduction in motor neuron counts in the CLN5 affected sheep spinal cord.

Fluorescent microscopy showed that lysosomal storage increased in the CLN6 affected sheep spinal cord from 3 to 18 months of age, whilst rates of accumulation were slower in CLN5 affected sheep until late in the disease course. Immunohistochemistry found that activated astrocytes were present in the CLN6 affected spinal cord at 18 months of age, but not in the ovine CLN5 model.

Collectively, these results show that pathological changes in the spinal cord occurred late in the disease process, making them secondary to that occurring in the brain. This indicates that CLN5 and CLN6 affected sheep may have a “top-down” or “brain-first” propagation of disease. Despite subtle differences in the pathogenic cascade, the pathological endpoint in the spinal cord for CLN5 and CLN6 affected animals was very similar. This natural history study of spinal cord pathology in ovine NCL increases our knowledge about disease progression and informs subsequent decisions on optimal routes of administration for gene therapy in NCL.

Keywords: Neuronal ceroid lipofuscinoses, Batten disease, Spinal cord, Sheep, CLN5, CLN6, Grey matter, White matter, Neurodegeneration, Lysosomal storage accumulation, Neuroinflammation, Glial activation, Gene therapy.

Acknowledgements

Sometimes the path you start on, leads you somewhere unexpected. It's these one-off encounters /sideroads that dramatically alter where you end up. This journey started for me when I first met Dr Sam, when she was lecturing into GENE 301, covering the use of animal models to study human diseases. This provided me with my first exposure to Batten disease. From there I found my side road, that's when I knew that my dreams and passion are in researching genetic animal models to study humans, and I was going to start with Batten disease as the concept had me intrigued.

Foremost, I must acknowledge Dr Nadia Mitchell as my supervisor. I want to thank her, not only for taking me on as a master's student, but for bringing me into the LU BARN team. Making sure to include me in all aspects of animal models for Batten disease, granting me the opportunity to get a fully rounded experience learning how the whole process works even though these tasks did not directly link into my project. Such as taking blood, culling (collecting brain, eyes, guts, spinal cords, etc samples for multiple different studies) and performing the OBDRS (Ovine Batten Disease Rating Scale) that monitors the disease's progression and the wellbeing of our sheep family.

I don't know how you do it Nadia but somehow you always make time for me, not only to talk about my project but also about anything that is happening personally. When it comes to explaining things to me you always find a way that makes sense to me, instead of a way that happens to work for someone else. I hope one day that I can balance my personal and professional life, as well as you do, with your confidence and grace.

I would also like to acknowledge Dr Samantha Murray as my co-supervisor, who may or may not have realized that she was my first exposure to this field of research, which resulted in me continuing into a master's degree. I particularly want to thank Sam for being there and taking the time to decipher my quick shorthand emails, answering my random questions, for the hours on the microscope discussing the cell morphology, and for allowing access to her natural descriptive thesaurus, and finally for all of the final proof reading.

In general, I want to thank everyone who is part of the LU BARN team, for welcoming me into the group, and always being there to lend a hand or ear, and demonstrating the required lab and sample collecting techniques. The LU BARN team is just like a family, as they care about each other, they are extremely dedicated to their work. Then on the flip side they are happy to sit and chat about anything and everything.

In addition to the LU BARN team, I also want to thank the extended BARN network as well for allowing me access to their extended knowledge, as well as to unpublished works. In particular, I want to thank Ashley Deane, Anila Pulickan, Madeleine Palmer, John Wynyard, and Martin Wellby (Lincoln University), Professor Jon Cooper (Washington University in St Louis, MO, USA), and Associate Professor Imke Tammen (University of Sydney, Australia).

I have to thank my Ohana. Especially my mum who has been my rock, always, there for me however I need her. Being there while I practice my orals, and telling me I can do it, even though I'm still so nervous that it's making me sick. For understanding that sometimes I just need to ring and de-stress when something hasn't worked out. My Dad, who always means well, and for all the previous years for proofreading my assignments through High School, and my BAgSci. And thank you to both of my grandfathers who were not able to even see me start university, but both of whom contributed financially to my education after they left us behind.

I also want to thank Rosemarie Richardson and the whole team at LU inclusive education. They deserve to know, their job is often thankless and even though their support was not necessary for the last few years, it was still their efforts through my BAgSci that made it possible for me to pursue my master's degree. I'm also incredibly thankful for being awarded the Inclusive Education Award (scholarship) this year (2022) as it made it possible to buy a new laptop with the capabilities for running all of the software and applications require to process my research data, reference my thesis, as well as run programs necessary as an inclusive education student.

Thank you to the LU gym, especially my boxing class ladies, who had taught me that **"Sometimes you just have to roll with the punches, and when you can't, throw in a hook"**.

Finally, I want to thank my friends, they know who they are. Thank you for understanding the radio silence which happens when I am deeply invested in a project, as it happens when I'm working on anything that I'm passionate about. I just have to work on it whenever I can, including weekends and weird hours to stay in the flow.

Sometimes the journey you go on isn't what you planned, but the people who take it with you make it all worthwhile, and I have loved my journey. It's been a little over a year and somehow it doesn't seem long enough!

“The greatest pleasure in life, is doing what people say you cannot do” - Walter Bagehot

Table of Contents

Acknowledgements	v
Table of Contents	viii
List of Tables	x
List of Figures	xi
Chapter 1 Introduction	1
1.1 NCL symptomology	1
1.1.1 Human CLN5 disease.....	2
1.1.2 Human CLN6 disease.....	2
1.2 Animal models of NCL.....	2
1.2.1 Small animal models	3
1.2.2 Large animal models	3
1.2.3 CLN5 and CLN6 sheep models.....	4
1.3 Brain pathology in NCL.....	6
1.3.1 Neurodegeneration.....	6
1.3.2 Neuroinflammation.....	6
1.3.3 Lysosomal storage.....	7
1.4 Therapeutic options for the NCLs	7
1.4.1 Therapy development in CLN5 and CLN6 sheep models	8
1.5 The spinal cord.....	8
1.5.1 Spinal cord anatomy	9
1.5.2 Spinal cord pathology in neurodegenerative diseases	12
1.5.3 Spinal cord pathology in NCL	14
1.6 Aims of this study.....	15
Chapter 2 General Materials and Methods	17
2.1 Animals.....	17
2.2 Tissues preparation and histology	17
2.3 Sectioning spinal cords	17
2.4 Nissl staining and area measurements	17
2.5 Quantification of lysosomal storage	18
2.6 Immunohistochemical staining.....	18
2.6.1 Neuronal staining.....	18
2.6.2 Astrocytic staining.....	19
2.6.3 Microscopy.....	19
2.7 Statistical analysis	19
2.8 Special methods.....	19
Chapter 3 Key pathological results in the ovine NCL spinal cord	20
3.1 Introduction	20
3.2 Sheep spinal cord area.....	21
3.3 Neuronal loss in the ovine NCL spinal cord.....	23
3.4 Lysosomal storage.....	26
3.5 Discussion.....	30

3.5.1	Area measurements.....	30
3.5.2	Neuron loss	31
3.5.3	Lysosomal storage.....	32
3.5.4	Trouble-shooting.....	33
3.5.5	Conclusion.....	34
Chapter 4 Neuroinflammation in the NCL spinal cord.....		35
4.1	Introduction	35
4.2	Materials and Methods.....	37
4.2.1	GFAP immunohistochemistry dilution series of thick 50 µm spinal cord sections....	37
4.2.2	GFAP Immunohistochemistry on thin 3 µm spinal cord sections	37
4.2.3	GFAP immunofluorescence on thick 50 µm spinal cord sections	37
4.3	Results.....	38
4.3.1	GFAP immunohistochemical dilution series	38
4.3.2	GFAP immunohistochemistry in thick 50 µm spinal cord sections.....	38
4.3.3	GFAP immunohistochemistry in thin 3 µm spinal cord sections	41
4.3.4	GFAP immunofluorescence in thick 50 µm spinal cord sections	43
4.4	Discussion.....	43
4.4.1	GFAP immunohistochemistry in thick 50 µm spinal cord sections.....	43
4.4.2	GFAP immunohistochemistry in thin 3 µm spinal cord sections	44
4.4.3	GFAP immunofluorescence in thick 50 µm spinal cord sections	45
4.4.4	Comparison with other NCL models	45
4.4.5	Conclusions	46
Chapter 5 Exploring other pathology in the NCL spinal cord		47
5.1	Introduction	47
5.2	Materials and Methods.....	49
5.3	Results.....	50
5.3.1	Parvalbumin expression in the sheep spinal cord.....	50
5.3.2	Calbindin expression in the sheep spinal cord.....	52
5.3.3	Calretinin expression in the sheep spinal cord	53
5.3.4	GSB4 expression in the sheep spinal cord	54
5.4	Discussion.....	55
5.4.1	Parvalbumin distribution in sheep spinal cord and other species.....	56
5.4.2	Calbindin distribution in sheep spinal cord and other species	56
5.4.3	Calretinin distribution in sheep spinal cord and other species.....	56
5.4.4	GSB4 distribution in sheep spinal cord	57
5.4.5	Comparison of interneuron and microglial expression patterns between control and affected sheep spinal cord.....	57
5.5	Conclusions	58
Chapter 6 Discussion and Conclusions		59
6.1	Spinal cord anatomy and neurochemistry in the healthy sheep spinal cord	59
6.2	Spinal cord pathology in the NCL affected sheep spinal cord	60
6.3	Comparison of spinal cord pathology, brain pathology and clinical symptoms in ovine NCL	62
6.4	Comparison with other NCL models	63
6.5	Implications for therapy.....	63
6.6	Future directions.....	64
References		65

List of Tables

Table 5.1	Primary and secondary antibodies used in this study	50
Table 5.2	Qualitative assessment of calcium binding protein immunoreactivity in the 18 month old healthy sheep cervical spinal cord.....	50

List of Figures

Figure 1.1	GPS tracking of sheep traversal in a closed field maze	5
Figure 1.2	A comparison of human and sheep spinal cord	9
Figure 1.3	A comparison of an adult human and adult sheep spine vertebrae	10
Figure 1.4	A schematic top view of the spinal cord.....	11
Figure 1.5	A cross-sectional view of the spinal cord at the cervical, thoracic and lumbar spine..	12
Figure 3.1	Regional differences in the healthy sheep spinal cord.....	22
Figure 3.2	Comparative spinal cord areas during ovine NCL disease progression.....	22
Figure 3.3	Regional differences between all genotypes in sheep spinal cord.....	23
Figure 3.4	Representative images of NeuN-positive motor neurons in the ventral horn.....	25
Figure 3.5	Motor neuron counts in the ventral horn during ovine NCL disease progression	25
Figure 3.6	Fluorescent microscopy of 50 μ m spinal cord sections.....	27
Figure 3.7	Accumulation of fluorescent storage bodies during ovine NCL disease progression ..	28
Figure 3.8	Fluorescent microscopy of 3 μ m spinal cord sections.....	29
Figure 3.9	Variation of the spinal cord width and depth for sheep and human	33
Figure 4.1	Early glial activation in CLN1 affected mouse spinal cords	35
Figure 4.2	GFAP-immunostained sections of white matter of the spinal cord in mice.....	36
Figure 4.3	GFAP dilution series	38
Figure 4.4	Astrocytosis in the spinal cord during ovine NCL disease progression	39
Figure 4.5	GFAP immunoreactivity during ovine NCL disease progression.....	40
Figure 4.6	Astrocytosis in the spinal cord grey matter during ovine NCL disease progression	42
Figure 4.7	Astrocytosis in the spinal cord white matter during ovine NCL disease progression ..	43
Figure 5.1	Cross-sectional view of the spinal cord	49
Figure 5.2	Parvalbumin immunoreactivity in the healthy sheep spinal cord.....	51
Figure 5.3	Calbindin expression in the healthy sheep spinal cord	53
Figure 5.4	Calretinin expression in the healthy sheep spinal cord.....	54
Figure 5.5	Summary of the control and affected immunohistochemistry staining	55
Figure 6.1	A timeline of clinicopathological changes in the CLN5 and CLN6 ovine NCL models...	62

Chapter 1

Introduction

Neuronal ceroid lipofuscinosis (NCL), also known as Batten disease, is a fatal inheritable neurodegenerative lysosomal storage disorder. The disease is primarily autosomal recessively inherited, thus affected individuals inherit two copies of the mutated gene (one from each heterozygous carrier parent). Heterozygous carriers are clinically healthy. The disease predominantly affects infants and children, with an estimated incidence of approximately 1 in 12,500 individuals worldwide [1]. Currently, there are 13 variants of NCL (CLN1-CLN8 and CLN10-CLN14), which have been classified by the age of onset and the affected *CLN* gene. This project focuses on two of these forms of NCL, CLN5 and CLN6.

NCL is characterized by progressive neurodegeneration, neuroinflammation, storage accumulation, and blindness [2]. It results in premature death and to date there is no cure [2, 3]. Although lysosomal storage accumulates in all cells of the body, the main affected organs are the brain and eyes hence therapeutic strategies have concentrated on them. However, the brain is not the only component of the central nervous system (CNS) which needs to be considered when assessing therapy options for NCL. The spinal cord serves vital motor, sensory and autonomic functions, and any pathology in it might need correction too.

Very little is known about NCL spinal cord pathology, except for some preliminary studies in CLN1/PPT1 knockout mice models [4]. The present study aimed to examine spinal cord pathology in CLN5 and CLN6 NCL sheep models. The variables analysed were the total, grey matter, and white matter area of the spinal cord, neuronal loss, glial activation/neuroinflammation and the accumulation of lysosomal storage bodies.

1.1 NCL symptomology

Clinical symptoms, which include progressive mental and motor deterioration, blindness, epileptic seizures, premature death, and age of onset from infancy to late adult, vary based on the variant of NCL [4]. Mutations in both the *CLN5* and *CLN6* genes result in a late-infantile form of NCL.

1.1.1 Human CLN5 disease

The human *CLN5* gene is located on chromosome 13 at position q21.1-q32, and to date 37 known mutations have been identified [5, 6]. These can be missense, nonsense, insertion, frameshift and/or deletion mutations. CLN5 affected patients usually become symptomatic between 4 and 7 years old [7, 8]. The initial symptoms include motor clumsiness, progressing to mental deterioration, visual impairment, ataxia, myoclonus, and epileptic seizures [8-10]. Vision loss occurs between the ages of 7 and 10 years, followed by premature death between 10 and 30 years of age [9, 11].

A less common adult CLN5 phenotype presents with the same symptoms, however the onset is in the late teens and patients only survive until their forties [12, 13]. A particular mutation p.Tyr374Cys has been identified in these later-onset CLN5 patients, the mutation appears to be a milder genetic mutation as it allows residual CLN5 function and thus results in symptomatic delay [12].

1.1.2 Human CLN6 disease

The human *CLN6* gene is situated on chromosome 15 q21-q23 [14] and to date 82 known mutations have been identified [5, 6]. The onset of CLN6 disease typically occurs between 3 to 8 years of age, by 4 to 10 years of age patients lose all motor skills and vision, and premature death occurs in their mid-20s [15]. Symptoms include seizures and motor difficulties presenting early, progressing to myoclonus and ataxia. This is accompanied by speech impairment, mental regression, and delayed visual impairment resulting in blindness [15].

Like CLN5, there is an adult onset CLN6 disease which is known as Kufs disease. Although the molecular basis of Kufs disease is unknown, genetic sequencing in three affected families revealed mutations in *CLN6* as the major cause of Kufs type A disease. Kufs disease is a later onset disease presenting with similar CLN6-like symptoms at around 30 years of age but with no visual impairment [16].

1.2 Animal models of NCL

An animal model is non-human species used in medical research to investigate a human disease. They are divided into large and small animal models and can then be split into four further categories. Orphan models occur in animals but have no equivalent in humans. Naturally occurring models of a human disease spontaneously exist within another species. Induced or experimental models attempt to reproduce human disease conditions via genetic engineering (knocking in or out genes or through the use of CRISPR/Cas9 gene editing), while negative or non-reactive models are normal disease-free control animals. Of these types, the most common and relevant animal disease models are genetically engineered and naturally occurring models [17].

Both small and large animal models of NCL exist. Animal models are essential for studying this disease. They have been invaluable in understanding the disease progression and pathology [18-20], and creating diagnostic tools and possible treatments [21], currently the most successful being gene therapies which will be discussed below.

1.2.1 Small animal models

Small animal models are commonly used when researching neurodegenerative genetic diseases prior to progressing to large animal models. The majority of small animal models are genetically engineered, most commonly by knocking-out the *CLN* gene of relevance resulting in a loss of the gene function and thus development of NCL disease. For example, yeast models are small organisms being utilized in CLN1, CLN2, CLN3, CLN10, and CLN12 studies, to examine cellular function in depth [22]. However, the most commonly used small animal models are rodent models, particularly mice models which have been used to further the understanding of disease pathology and possible treatments for NCL.

There are 14 NCL mouse models in existence, including two knock-out models for adult onset CLN13 and CLN4 disease. The 12 remaining are early-onset models of CLN2,5,6,7,8, and 10, with two CLN1 models and four models of CLN3. The use of multiple models increases understanding of the disease as there are subtle and obvious differences between them. In particular, this is seen with the four CLN3 mice models, as different mutations in the same gene resulted in differences in age and neurological symptom onset, ranging from less than two months up to 16 months [22].

Mice and rats are easy to handle, highly reproductive, and cheap to house, however, they have less similarity on a genetic, anatomical and physiological level to human patients than larger animal models [22].

1.2.2 Large animal models

There are numerous naturally occurring larger animal NCL models that have been identified and utilized ever since the first was discovered in 1953 in a setter dog [22, 23]. The most notable significant models to date have been in *Ovis aries* (domestic sheep) and *Canis lupus familiaris* (domestic dog). NCL has also been reported and studied in cattle, horses, pigs, goats, cats, ferrets, birds, and monkeys [22]. These large animals models have increased the understanding of NCL pathophysiology and affected animals have been utilized in the development and efficacy testing of enzyme replacement and gene therapies for NCL [22].

1.2.3 CLN5 and CLN6 sheep models

Two naturally occurring sheep models at Lincoln University have been used in this project. These are in Borderdale and South Hampshire sheep breeds which are models for CLN5 and CLN6 disease respectively.

The CLN5 sheep model was discovered in 2002 in New Zealand Borderdale sheep, through a veterinarian observing NCL – like symptomology, starting with visual deterioration, in a flock of sheep at Dunsandel, Canterbury [24]. Subsequent genetic sequencing established the disease causing mutation, a substitution at splice site (c.571+1G>A) which results in the excision of exon 3 and a truncated putative CLN5 protein [25]. A flock of sheep were then established from sheep heterozygous for this mutation.

The New Zealand South Hampshire sheep was first identified in 1976 as having a naturally occurring CLN6 disease variant [26-28]. The disease-causing mutation is a 401bp deletion in the 5' region of the *CLN6* gene but this has not yet been published (Nadia Mitchell, personal communication). Of note, a naturally occurring form of CLN6 NCL also occurs in Australian Merino sheep and these animals also remain under active study [29-31].

Both the Borderdale CLN5 and South Hampshire CLN6 sheep are excellent models of the human disease and share extensive similarities in clinical progression and pathology to affected patients. Diseased sheep present normally/ asymptomatic at birth, however neuroinflammation (glial activation) and lysosomal storage is already evident in their brains [32-34].

By 6 months of age, deterioration of the brain is occurring. The initial and most substantial neuron and volume losses occur in the parieto-occipital and visual cortices but spread across the entire cortical mantle by end stage-disease [34, 35].

Clinical symptomology is apparent by 9 months of age, with behaviours including star-gazing or tilted heads due to visual defects observed by reduced electroretinograms [36] and lost or reduced menace responses [35].

With time, affected sheep show unsettled wandering, circling, affected gait, and self-isolation [35]. Seizures, particularly in the CLN6 affected sheep, diminish their activity level and reduce their mental capacity. Stress can increase their seizure frequency and panic running (while visually impaired).

Cognitive maze tests reveal disease-associated changes over time. Healthy control CLN5 heterozygous (*CLN5*^{+/-}) sheep consistently follow a uniform track through a maze. In contrast, CLN5

affected ($CLN5^{-/-}$) sheep take a longer and less uniform path at 8 months and by 19 months they compulsively circle at the start or are too affected to participate (Figure 1.1) [37].

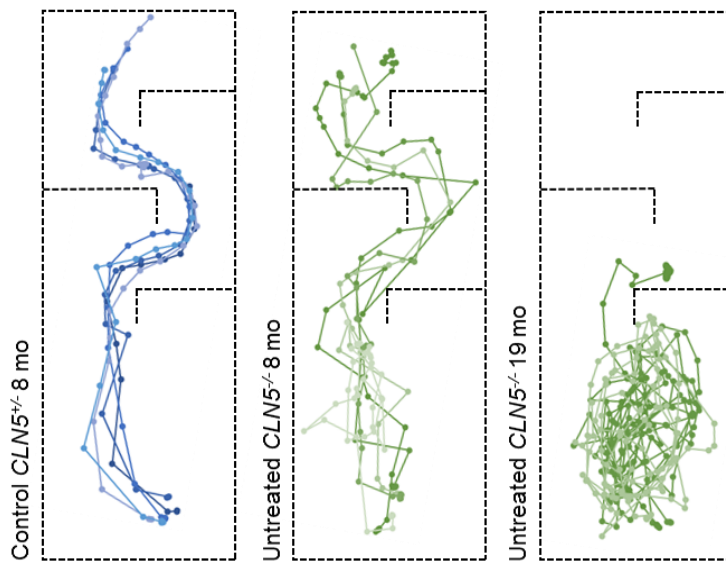


Figure 1.1 GPS tracking of sheep traversal in a closed field maze

Sheep were tracked during five traversals through a maze. Each individual line represents an individual traversal. Healthy control sheep (blue) followed a uniform path over their lifetime, whilst $CLN5$ affected sheep took a longer and less-uniform track. By 19 months of age, affected sheep simply circled in the start area and were unable to complete the task [37].

By 24 months, neuropathological studies show that few large cortical neurons remain in the affected sheep brain and their cognitive decline and behavioural changes result in premature death / humane euthanasia [35].

Sheep models have many advantages over smaller NCL animal models. The disease is a neurological disorder and sheep have increased brain size and more comparable neuroanatomy to humans. Brain weight is 1300-1400g, 130-140g, 2g, and 0.5g for adult humans, sheep, and rat and mice rodent models respectively [38]. The larger sheep brain allows reasonable extrapolation of an accurate drug-safe volume of any therapy and translatable delivery systems to treat the human brain.

Sheep are also similar in weight to humans, weighing 3.5–4.5 kg at birth and growing to 80 to 110-kg as adults [37]. The lifespan of sheep at 12-15 years is also significantly longer compared to rodents at 2-3 years [38], which is essential to observe the long-term effects and efficacy of a therapy. Sheep are docile animals thus allowing various sample collections and handling to be carried out with limited stress. Additionally, flocks are housed outdoors, thus are easy to care for and maintain. There are also spinal cord similarities between sheep and humans, first noted in the 1970s discussed further in Section 1.5 [39, 40].

1.3 Brain pathology in NCL

Brain pathology in NCL revolves around neurodegeneration, neuroinflammation, and lysosomal storage body accumulation [2]. Because neuropathology studies in humans are often limited to postmortem brains collected at a terminal disease stage, animal models of NCL have been instrumental in determining the pathophysiology of the disease and the sheep models have been particularly informative.

1.3.1 Neurodegeneration

The most common pathological feature of NCL is severe neurodegeneration or neuronal loss, which results in brain atrophy (shrinkage) [2]. Neurons are nerve cells that utilise electrical impulses and chemical signals, to receive and transport sensory messages from the body to the CNS and in particular the brain. Neurons consist of a cell body, dendrites, and axons (extensions of the cell body) which transmits messages from the cell. Dendrites receive messages from the axons of adjacent neurons, through the synapse in the form of chemical neurotransmitters.

Magnetic resonance imaging (MRI) and postmortem analyses show that not all brain regions are affected by neurodegeneration in the NCL affected patient. Instead, it is selective regions and selective neuronal populations that are thought to be affected. In ovine CLN5 and CLN6 disease, gross atrophy of the cerebral cortex occurs from 6 months of age [41], with a reduction in cortical thickness first apparent in the visual and parieto-occipital cortices, the regions first associated with clinical symptomology [34, 35]. Cortical regions, like the motor cortex, are less affected and there is very little neuronal loss in subcortical structures and the cerebellum, even at end-stage disease [34, 35].

1.3.2 Neuroinflammation

Glial cells (neuroglia) are the non-neuronal cells of the CNS. They are essential for providing physical structure to support neurons, as well as providing nutrients, and being involved in waste transport and signaling. There are three key glial cells – astrocytes, microglia and oligodendrocytes. After CNS trauma, infection or in neurodegenerative diseases, glial cells can become activated [42]. Activated glial cells have an altered morphology, their cell body increases in size and their branches thicken and have a shorter reach. They can upregulate the synthesis and secretion of certain chemicals (cytokines and chemokines), stimulating a complex neuroinflammatory cascade [42].

Neuroinflammation is an inflammatory response that is observed in the brain or the spinal cord. There are two types of neuroinflammation, positive and negative. Positive neuroinflammation is a brief and controlled inflammation, providing benefits such as tissue repair, enhanced plasticity, and

neuroprotection [43]. However high levels of inflammation can result in negative aspects including neuronal damage, cognitive impairment, collateral damage, and anxiety and depression [43]. This introduction will focus on these negative aspects which are the result of chronic and uncontrolled inflammation, typically caused by traumatic CNS injury and neurodegenerative diseases like NCL.

An increase in neuroinflammation has been seen to occur with normal aging, multiple neurodegenerative diseases and is also associated with depression, a common consequence of neurodegenerative diseases [44]. Chronic inflammation results in extended activation of microglia (immune cells of the CNS), and this activation is sustained by the release of inflammatory oxidative and nitrosative stress, which is further detrimental for neurodegenerative diseases [44].

In ovine CLN5 and CLN6 disease, neuroinflammation or glial activation was found to be progressive, regionally specific, and a precursor of neurodegeneration in the brain, with neuroinflammation even being present in affected sheep foetuses [32, 34, 35]. As such, neuroinflammation in the NCL brain can be used as a predictor for neuronal loss [34].

1.3.3 Lysosomal storage

Intracellular storage body accumulation is a feature of NCL, and is observed early and in all forms of NCL [34]. Affected cells become distended with the accumulation of storage bodies [34], although the dysfunction caused by this increased storage varies and is still unknown. Some neuronal cells that have increased storage die, whilst others like the Purkinje cells of the cerebellum can have significant storage burden but do not die - this is a common aspect of human NCL and animal models [45]. In sheep and mice models, the increased storage occurs predominantly in neuronal cells in the brain [34]. In ovine CLN5 and CLN6 disease, the accumulation of storage material is evenly spread across the regions in the brain and follows a linear pattern increasing with age [34, 35]. However, most other cell types throughout the body accumulate storage bodies as well [46], although there is no evidence of its function outside the brain on the cellular or physiological level [46].

1.4 Therapeutic options for the NCLs

NCL is a fatal disease and to date there is no cure. One of the most promising therapeutic options is gene therapy. Gene therapy allows correction of a mutated gene or site-specific modification, by delivering a functional copy of the affected gene [47]. The functional gene is inserted into a delivery vector, which is either a plasmid, nanostructure or naked virus [47]. It is essential that the vector has the packaging capacity to hold the necessary gene, is not recognized by the immune system, and can be purified in large quantities and high enough concentrations to make it commercial viable [47]. Adeno-associated viral (AAV) vectors are the current preferred choice in gene delivery for the treatment of a variety of human diseases. AAV does not cause any human disease and was approved

in 2017 for human clinical trials by the United States Food and Drug Administration (FDA) [48]. AAV vectors have the capacity to package up to 4.6kB of DNA, do not integrate into the recipient genome (therefore the gene therapy will not permanently alter the individual's genome), and have only a mild inflammatory response compared to other viral vectors [47].

1.4.1 Therapy development in CLN5 and CLN6 sheep models

These two models have also been utilised in the development of gene therapies. Gene therapy has been used to replace the defective NCL genes in both South Hampshire (*CLN6^{-/-}*) and Borderdale (*CLN5^{-/-}*) sheep [49]. The brain-directed gene therapy is delivered via an intracerebroventricular route, into the cerebrospinal fluid (CSF) in the lateral ventricles. This resulted in transduced cells, that had taken up the virus and were expressing the *CLN5* or *CLN6* gene, throughout the brain and along the full extent of the spinal cord [50].

The *CLN5* gene therapy has produced some very encouraging results. Intracerebroventricular administration of an AAV serotype 9 (AAV9), was able to prevent or halt brain atrophy and cognitive decline in both pre- and post-symptomatic *CLN5^{-/-}* sheep [37, 50]. However, treated sheep still lost their vision [37]. To address this, in a separate study, *CLN5* affected sheep received AAV9-mediated *CLN5* gene therapy via intravitreal delivery, into the vitreous humour of one eye [51]. The other eye served as an internal untreated control. This treatment was able to attenuate retinal dysfunction and pathology in the treated eye. In September 2021, the candidate *CLN5* gene therapy product was cleared as an investigational new drug by the FDA, based on data carried out on *CLN5^{-/-}* Borderdale sheep in New Zealand [37, 49, 50, 52].

Biotechnology company Neurogene Inc funded these most recent gene therapy trials and sponsored the FDA application. They are currently enrolling patients into a Phase I/II *CLN5* gene therapy clinical trial for *CLN5* patients utilising both the intracerebroventricular and intravitreal delivery routes [53] (ClinicalTrials.gov identifier NCT05228145 [54]). This trial is a non-randomized open-label study. Selected participants will be 3- to 8-year-old children with *CLN5* disease, exhibiting impaired language and impaired visual acuity or impaired motor function [54]. Each participant will be followed for 5 years after initial treatment for safety and efficacy and evaluation of their motor, language, visual and cognitive function [54].

1.5 The spinal cord

Whilst gene therapy looks to be correcting or slowing the neurological component of NCL, the brain is not the only structure in the CNS which may need correction. Pathology can also be seen in the spinal cord in other neurodegenerative diseases.

1.5.1 Spinal cord anatomy

The spinal cord is separated into four regions: cervical, thoracic, lumbar, and sacrum (Figure 1.2). It is surrounded by the spinal column, which is comprised of vertebrae. Similarities between the sheep and human spine were first noted in the 1970s [39, 40]. A comparison of the number of vertebrae in each region is very similar, with sheep having 7 cervical, 12-14 thoracic, 6-7 lumbar, and 4 sacral vertebrae while humans have 7, 12, 5, and 5 respectively (Figure 1.2). This means that the overall



Figure 1.2 A comparison of human and sheep spinal cord

A. The human spine with numbered vertebrae. The seven cervical vertebrae are pink, while the 12 thoracic vertebrae are pale blue, the 5 lumbar vertebrae are green, and the yellow section is the 5 fused vertebrae of the sacrum. B. The sheep spine similarly numbered and colour-coded. Figure A modified from <https://johnhawks.net/the-different-types-of-vertebrae-in-the-human-spine/> and Figure B modified from <https://quizlet.com/303292251/sheep-skeletal-system-diagram/>.

Figure 1.2 also demonstrates the anatomical difference between the vertical human (bipedal) spine and the horizontal sheep (quadruped) spine. Most anatomical research has focussed on the skeletal structure of the spinal cord, in particular the dimension of vertebrae parts, including but not limited to the vertebral body, canal width and depth, and pedicles [55]. Anatomically, the structure of the vertebrae is the same although the overall size of the sheep vertebrae is smaller (Figure 1.3). In both species the spinal canal, and therefore the spinal cord, is the widest and deepest at the cervical level, narrowing through the thoracic region and then increasing into the lumbar spine (Figure 1.3), and at all regions the sheep spine is between 50-78.8% and 44-74% of a human spine for the canal width and depth respectively [55, 56].

Material removed due to copyright compliance

Figure 1.3 A comparison of an adult human and adult sheep spine vertebrae

The number of vertebrae and the canal width and depth, at the cervical, thoracic and lumbar regions. Data sourced from [55].

The spinal cord fits within the vertebral foramen also called the spinal canal (Figure 1.4). Like the brain, it is surrounded by three meningeal layers – the dura mater, arachnoid mater and the pia mater. CSF flows between the arachnoid and pia mater layers. There are 31 symmetrical pairs of nerves in humans, which connect the spinal cord to the periphery [57]. These nerves are split up across the different regions of the spinal cord, with one pair of nerves per vertebra [57].

Each of the spinal nerves has dorsal and ventral roots (Figure 1.4). The dorsal root contains the sensory fibres from the neurons in the dorsal root ganglia and these fibres convey information from the peripheral visceral and somatic structures [57]. Ventral roots of the spinal cord contain the motor fibres of the anterior motor neurons, which pass signals to the skeletal muscles [57]. The motor neuron cell bodies reside in the ventral horn of the spinal cord grey matter.

Material removed due to copyright compliance

Figure 1.4 A schematic top view of the spinal cord

This cross-sectional diagram shows a single spinal vertebra, with the ventral and dorsal horn, ventral root and dorsal root ganglion, white and grey matter, meningeal layers and vertebral body labelled. Figure modified from <https://quizlet.com/274761396/cross-section-of-spinal-cord-and-vertebra-diagram/>.

There is a difference in the vertebrae size in the cervical, thoracic, and lumbar spine and this is reflected in the overall spinal cord size and therefore also the distribution of grey matter and white matter (Figure 1.5).

The spinal cord sections consist of white and grey matter. The white matter surrounds the grey matter and is packed full of both ascending and descending axons extending between the spinal cord and the brain [58]. The grey matter is a butterfly shape which varies in shape and overall size over the length of the spinal cord (Figure 1.5). It is made up of nerve cells, glial cells and blood vessels [58]. The main cells are motor and sensory neurons and connecting interneurons.

Material removed due to copyright compliance

Figure 1.5 A cross-sectional view of the spinal cord at the cervical, thoracic and lumbar spine Specifically, the human C5, T8, and L3 (from left to right). The pale yellow is the white matter of the spinal cord while the darker orange (butterfly shape) is the grey matter. Created with BioRender.com

The grey matter consists of dorsal and ventral horns; the dorsal horn at the posterior end of the spinal cord receives all of the sensory information that enters via the dorsal roots [59]. Thus the dorsal horn is primarily composed of sensory neurons and interneurons that receive information from somatic and visceral sensory neurons [60]. The ventral horn at the anterior of the spinal cord is comprised of visceral motor neuron and somatic motor neuron [60] cell bodies, which sends axons via the ventral roots to terminate on striated muscles [59].

1.5.2 Spinal cord pathology in neurodegenerative diseases

Examination of the literature indicates that many different animal models of neurodegenerative diseases have been used to study brain and spinal cord pathology. Three particular case studies in animals are presented below.

Hereditary Canine Spinal Muscular Atrophy (HCSMA) is a neurodegenerative disorder in dogs, which affects the upper (brain) and lower (spinal cord) motor neurons, and is clinically and pathologically similar to human motor neuron disease [61]. This canine model permits investigations early in the disease when there are still viable motor neurons, which could possibly be responsive to therapies. HCSMA, like human motor neuron diseases, is inherited as an autosomal dominant condition. Both diseases result in progressive weakness and atrophy of the proximal muscle groups with fasciculations, fibrillations, and sparing of oculomotor muscles and vesicorectal sphincters.

Affected dogs are diagnosed by muscle biopsy and are categorised as having an accelerated, intermediate or chronic form of the disease [61]. The spinal cord of intermediate-stage HCSMA dogs has been examined – ventral horn neurons in the cervical region were enlarged, whilst there were 25% less neurons and the axonal diameter and area of the roots were smaller compared to the age-matched controlled dogs [61].

Amyotrophic lateral sclerosis (ALS) is a group of fatal human neurodegenerative diseases characterized by progressive motoneuron loss. It is characterized by a late-adult onset and rapid progressive loss of muscle function, starting with strength reduction and progressing to paralysis and loss of essential functions such as breathing and swallowing, thus resulting in death [62]. ALS symptoms are caused by a loss of both upper and lower motor neurons and accumulation of intracellular protein aggregates [63]. Interestingly, the major component of these aggregates is a 43-kDa transactive response DNA-binding protein (TDP-43), which is found in the insoluble fraction of both patients with sporadic ALS and frontotemporal lobar degeneration [63].

Non-human primate and rodent models of sporadic ALS exist [63-66] and the former best recapitulates the TDP-43 proteinopathy and has been instrumental in discovering key features of it [63]. Patients with ALS have more diffuse cytoplasmic TDP-43 in the spinal cord than in the brain. However, in the spinal cord of primates, neither C-terminal nor phosphospecific TDP-43 antibodies have been able to detect the 25-kDa C-terminal fragment that is found in patients with ALS [63]. It is possible that small amounts of C-terminal truncated are present but have not been identified because of mislocalization of the TDP-43. TDP-43 was detected in most large neurons of the primate thalamic lateral nuclear group – a brain region heavily involved in motor control - early in the disease course and these motoneurons later showed neuron loss [63].

Degenerative myelopathy (DM) is another degenerative spinal cord disease. It naturally occurs in dogs and the canine disease is similar to a form of ALS associated with superoxide dismutase 1 gene (*SOD1*) mutation [62]. There are 150 different *SOD1* mutations that have been associated with ALS and a mutation in one of the two *SOD1* alleles results in ALS.

DM occurs in many dog breeds, and typically has an onset of ~9 years in large breeds and ~11 years in Pembroke Welsh Corgis. Cervical spinal cord and associated spinal nerve roots, the ulnar nerve, and the extensor carpi radialis (ECR) muscle have been analysed from early and late-stage DM Corgis and age-matched control dogs [62]. Early in the disease, clear muscle changes were apparent yet the number of motor neuron cell bodies, axons in the motor or sensory nerve roots, or in the ulnar nerve did not change, even at late-stage disease [62]. In affected dogs, the lower motor neurons remain morphologically intact even with relatively advanced clinical signs [62]. This shows that changes in muscle fiber type and size occur early in the disease progression, thus therapies should focus on these, with a secondary focus on motor neurons and sensory neurons [62].

These three case studies reveal that brain and spinal cord pathology can vary within a neurodegenerative disease model. Therefore, understanding spinal cord pathology could affect how, where and when the disease can be treated, quite independent of what is seen in the brain.

1.5.3 Spinal cord pathology in NCL

Little is currently known about NCL spinal cord pathology, except what has been found in mice models, and one unpublished study carried out on CLN6 affected Merino sheep. No published spinal cord pathology research has been carried out in larger animal models or for *CLN5* and *CLN6* sheep models. A spinal cord pathology study will increase information about NCL disease progression, including when and where the first signs of the disease manifest (in the brain or spinal cord). This order of disease progression may influence possible treatments and further research.

1.5.3.1 Spinal cord pathology in NCL mice

The only published studies assessing spinal cord pathology in NCL were carried out on CLN1 affected mice. These mice have a mutation in the *CLN1/PPT1* gene which codes for a soluble lysosomal protein, palmitoyl protein thioesterase I (PPT1), and hence are termed Ppt1– deficient (*Ppt1*^{-/-}). CLN1 affected mice share most of the human phenotypic traits exhibited in *CLN1* patients, including reduced lifespan, visual defects, epileptic seizures and increasing gait defects as the disorder progresses [4, 67]. The first study performed by Shyng et al (2017) examined neuron loss, accumulation of autofluorescent storage material and glial activation in CLN1 affected mice at 1,3,5 and 7 months of age [4].

Neuron loss is a characteristic hallmark of CLN1 disease, with significant loss seen in the cerebellum and thalamus of CLN1 affected mice by 5 months, while significant neurodegeneration was actually observed earlier in the spinal cord. Neurons were lost as early as 3 months of age in the cervical, lumbosacral dorsal horn, and thoracic ventral horn of the spinal cord [4, 68]. From 5 months of age onwards, all regions of the affected spine had significant neuron loss in both the dorsal and ventral horns [4, 68].

Autofluorescent storage material was present at 3 months of age in the cell bodies within the spinal grey matter of the dorsal and ventral horns of CLN1 affected mice [68], although the burden level then stayed constant between 3 and 7 months of age [4].

Activation of glial cells (astrocytes and microglia) is associated with neuron loss in the forebrains of CLN1 affected mice, preceding neurodegeneration [69]. A recent study revealed that microglial activation was present in the affected mice brain at 1 month of age and prior to significant interneuron loss [68]. At 3 months the CLN1 affected mouse brain displayed a dramatic increase in the intensity of CD68 staining, which is a marker of microglial activation, thus revealing morphological changes of microglia to brain macrophages [4]. Also at this same age, immunostaining of the spinal cord with an astroglial marker, glial fibrillary acidic protein (GFAP), showed increases in hypertrophied astroglia in the grey matter, which then became completely filled with activated

astrocytes from 5 months of age. Interestingly the number of activated astrocytes in the spinal white matter didn't increase until 5 months onward [4].

These studies concluded that neuron loss in the CLN1 affected mice spinal cord was observed two months prior to being seen in the cerebellum and thalamus, which occurred at 5 months. Equally glial cell activation occurred earlier in the CLN1 affected mouse spinal cord than in the brain and started in the grey matter.

1.5.3.2 Spinal cord pathology in CLN6 sheep

An unpublished study has been performed in Australian Merino sheep with naturally occurring CLN6 NCL [70]. A systematic histopathological analysis of neuronal degeneration and necrosis, gliosis, lysosomal storage burden and demyelination level was performed on 12 *CLN6*^{-/-} sheep aged 14 – 17 months of age, and compared to data collected from three 42-month-old healthy control sheep. Formalin-fixed spinal cord sections from the cervical, thoracic and lumbar regions were paraffin embedded, sectioned and stained with hematoxylin and eosin. The five pathological characteristics were graded from 0 (not present, within normal limits) to 3 (marked presence) in three random microscope fields in the white and grey matter, for both the dorsal and ventral horns of the spinal cord.

As expected, lysosomal storage was not present in the control sheep spinal cord but significantly increased in both the dorsal and ventral horns of the affected sheep spinal cord [70]. Interestingly, there was less gliosis in the white matter of the affected sheep than controls, which contradicted the heightened neuroinflammation seen in the CLN1 diseased mouse grey and white matter [4]. There was a gradient pattern of neuronal degeneration and necrosis in the CLN6 affected sheep spinal cord, with greater severity in the cervical region than the lumbar [70]. This would suggest a rostral-caudal spread of pathology from the brain to the lower spinal cord in the CLN6 affected sheep that is quite unlike the CLN1 mouse model, where pathology occurs earlier in the spinal cord than the brain [4, 18, 68].

1.6 Aims of this study

This study aimed to investigate spinal cord pathology in CLN5 and CLN6 sheep models, by measuring the total spinal cord area, grey matter area, white matter area, neuron loss, lysosomal storage accumulation and glial activation.

A number of hypotheses were tested:

Area measurement hypothesis: Quantification of total, grey and white matter areas in the spinal cord will show reductions over time in affected sheep, compared to age-matched healthy sheep, due to neuron loss in the diseased spinal cord.

Autofluorescent storage material hypothesis: Progressive accumulation of autofluorescent storage material will occur in grey matter neurons of the diseased spinal cord, much as it does in the brain.

Glial activation hypothesis: Glial activation will occur early in the ovine NCL disease course and this will progressively increase over time.

Drawing comparisons to the CLN1 affected mouse model, it was hypothesised that neurodegeneration and other disease pathology will also be observed in the affected sheep spinal cord. However, the preliminary studies in CLN6 affected Merino sheep suggest this may not be the case. An interesting aspect of this study will be seeing if this occurred earlier in the spinal cord than in the brain, as seen in affected mice, or not.

The pathophysiology of spinal cord degeneration is essential to add to the particulars known about NCL disease models. The additional research can be utilised in decisions made around treating the NCL diseases, as well as whether spinal pathology contributes to the clinical progression already observed in large animal NCL models.

Chapter 2

General Materials and Methods

2.1 Animals

The CLN5 and CLN6 NCL disease models used in this study are in Borderdale and South Hampshire sheep breeds respectively. At 3,6,9,12,15 and 18 months of age, at least two healthy control (heterozygous) sheep of each breed and at least two *CLN5* affected (*CLN5*^{-/-}) and two *CLN6* affected (*CLN6*^{-/-}) sheep were sacrificed by penetrating captive bolt between the cervical (C3-C4) vertebrae followed by immediate exsanguination. All animal procedures complied with the New Zealand Animal Welfare Act (1999), and National Institutes of Health guidelines, and were performed under the approval of the Lincoln University Animal Ethics committee (2017-40 and 2020-22).

2.2 Tissues preparation and histology

The spinal column was separated from the connective tissue and a 10 cm centimetre section was collected from each of the three regions (cervical, thoracic and lumbar). A blunt object was used to remove the spinal cord from the vertebral canal. Spinal cord samples were then fixed in 10% formalin in 0.9% NaCl at 4°C. After a week, the spinal cord samples were cut into 1 cm samples and placed into equilibration solution (20% sucrose, 10% ethylene glycol, and 0.9% NaCl) for a further week or until the sample sunk. The spinal cords were then briefly dried, wrapped in foil and frozen at -80°C, awaiting sectioning.

2.3 Sectioning spinal cords

Spinal cords were sectioned using an HM 430 microtome (Microm International GmbH, Walldorf, Germany), set to 50 µm, on a stage mount which was frozen prior to use. The spinal cord sample was fixed to the stage mount using Shandon cryomatrix frozen embedding medium (Thermo Scientific, USA) and powdered dry ice, and then placed in the -20°C freezer for 10 minutes prior to sectioning. Sections were collected and stored (6 sections per well) within a 96 well plate containing cryoprotectant (30% ethylene glycol, 15% sucrose, 0.05% sodium azide in phosphate buffered saline, pH 7.4) and stored frozen at -20°C until histological processing.

2.4 Nissl staining and area measurements

To analyse area measurements and look for neuronal structure and histological abnormalities, spinal cord sections were mounted onto slides in chrome alum solution (0.5% gelatine and 0.05% chromium potassium sulphate) and allowed to air dry overnight. The slides were then passed through an

ethanol gradient, equilibrated in water and incubated in Nissl solution (0.05% cresyl violet acetate, 0.05% acetic acid in water) for 10 minutes at 37°C and rinsed in water. Slides were dehydrated, cleared in xylene and coverslipped with DPX (Dibutylphthalate Polystyrene Xylene, BDH, Poole, England). Both Nissl and GFAP stained sections were used to measure the total, grey and white matter areas as both stains provided a distinct grey-white matter boundary. The intact spinal cord sections were imaged and cross-sectional area calculations were determined using ImageJ (version 1.53k) National Institutes of Health (NIH, Bethesda, MD, USA). The drawing tool was used to calculate the total area of the spinal cord and the grey matter area, allowing the white matter area to be calculated, using the equation: White matter area = Total area – Grey matter. Area calculations were made from at least 5 spinal cord sections, for each of the three spinal cord regions, per animal at each age.

2.5 Quantification of lysosomal storage

To look for fluorescent lysosomal storage, 4-6 sections of the spinal cord per region per animal were mounted onto slides using chrome alum solution, air-dried, and then cover-slipped with glycerol. The sections were examined under a Nikon Eclipse 50i fluorescent microscope (Nikon Instruments Inc., Japan) and ten .jpg images in the dorsal and ventral spinal columns were collected. The images then underwent thresholding image analysis using ImageJ to determine the number of pixels with a fluorescent brightness level above a set threshold which was expressed as the percentage area of fluorescence.

2.6 Immunohistochemical staining

2.6.1 Neuronal staining

Spinal cord sections were stained with a neuronal marker, NeuN (Rabbit anti-NeuN, 1:500, ab177487, Abcam, Cambridge, UK) using established methods [34]. In brief, sections were pre-incubated in 1% H₂O₂, 30 min, blocked with 10% normal goat serum (Invitrogen, Carlsbad, CA, USA) in phosphate buffered saline (PBS) containing 0.3% Triton X-100 (PBST), 2h, followed by incubation in the primary antibody for 60 hours at 4°C. Immunoreactivity was detected with a goat anti-rabbit IgG biotinylated secondary antibody (1:1000, B7389, Sigma-Aldrich, Australia) for 4 hours at room temperature, followed by Extravidin – Peroxidase conjugate, 1:1000 (E2886, Sigma-Aldrich) for 2 hours and then incubation for 7 minutes in 0.5 mg/ml diaminobenzidine tetrahydrochloride (DAB, D5637, Sigma-Aldrich) containing 0.01% H₂O₂ in PBS [34]. Sections were mounted in chrome alum solution, air-dried, and then cover-slipped with DPX.

2.6.2 Astrocytic staining

Spinal cord sections were also stained with an astrocytic marker, glial fibrillary acidic protein (GFAP). The immunohistochemical protocol was the same as described above for NeuN, except the primary antibody was rabbit anti-cow GFAP (1:10,000, Z0334, polyclonal, Dako, Ely, England).

2.6.3 Microscopy

Ten images of NeuN and GFAP stained sections in the dorsal and ventral spinal columns were taken on the Nikon Eclipse 50i microscope. The microscope lamp intensity, exposure time and use of neutral density filters were kept constant for capturing all images for each immunostain. Cell counts were determined from the NeuN images using ImageJ. Images were thresholded to capture NeuN-positive cells only and automated counting was performed using the analyze particles function to capture cells with a diameter $\geq 30 \mu\text{m}$. The GFAP images underwent thresholding analysis through ImageJ, as detailed above for lysosomal storage quantification, to determine the percentage area of immunopositive cells.

2.7 Statistical analysis

Statistical analyses were performed on GraphPad Prism© software (GraphPad, La Jolla, CA, USA). Means (total area, total neuron counts, % area fluorescent or % area stained) and the corresponding standard deviation (SD) and standard errors of the mean (SEM) were computed for each spinal cord region for each animal. These means were used in a one-way ANOVA (Brown-Forsyth and Welsh) to test each region separately for differences between control and *CLN6*^{-/-} or *CLN5*^{-/-} sheep. If a significant difference was detected, then multiple unpaired t-tests assuming unequal variances using a false discovery approach (Welsh t-test) were performed to test for differences between genotypes at each age. Differences were considered as statistically significant where $P < 0.05$.

2.8 Special methods

Additional special methods relating to particular experiments are included in the appropriate chapter.

Chapter 3

Key pathological results in the ovine NCL spinal cord

3.1 Introduction

Neurodegeneration and lysosomal storage are the key defining pathological observations in the NCL brain yet much less is known about them in the spinal cord. This chapter presents a detailed study of these two pathologies in the ovine CLN5 and CLN6 disease models. Histopathological and magnetic resonance imaging studies in CLN5 affected (*CLN5*^{-/-}) and CLN6 affected (*CLN6*^{-/-}) sheep have shown significant atrophy is observed in the cerebral cortex, while minimal volume loss or neuronal loss is observed in the subcortical structures and cerebellum [34, 35, 71]. Conversely, lysosomal storage occurs in most cell types throughout the body and is present as early as birth in affected sheep brains, but is evenly distributed and increases linearly with age [34, 35].

Atrophic changes in the brain can be calculated by area or volumetric analyses, using techniques such as stereology or neuroimaging [33, 41, 71, 72]. Similarly, total cross-sectional area, and grey and white matter area calculations at the cervical, thoracic and lumbar spinal cord levels have been used to quantify potential atrophy in the spinal cord [18, 68, 73]. The spinal grey matter is largely composed of neuronal cell bodies and some unmyelinated axons and these cells are involved in muscle movement and sensory transmission. Given that the main driver of atrophy in the affected sheep brain is neuronal loss in the grey matter, it is anticipated that any neurodegeneration in the CLN5 and CLN6 affected sheep spinal cord would also reduce grey matter and total area measurements, a phenomenon that has been observed in mice with CLN1 NCL [18, 68].

Immunohistochemistry can also be used to investigate neurodegeneration. NeuN is a soluble nuclear protein, which is commonly used as a biomarker for neurons. A monoclonal antibody to the NeuN protein is able to bind to almost all neuronal cell types of both the central and peripheral nervous system, including small interneurons such as those in the spinal cord and cerebellar granule cells. Therefore, NeuN-based cell counting can be used to assess neuronal loss in neurodegenerative diseases and other disorders [74, 75].

The dorsal and ventral horns of the spinal cord are composed of different neuronal populations. The dorsal horn is mainly composed of unipolar sensory neurons and small, uniform, circular interneurons. In comparison, the ventral horn is comprised of motor neurons, which control muscle movement through projection of their axons into the periphery to innervate skeletal muscle. Motor neurons are significantly larger than sensory neurons and vary in shape. Because of the different spinal cord neurons and morphologies, neuronal counts need to be analysed in the two horns of the

spinal cord separately to accommodate for the different sizes and shapes. Since NCL is a neurodegenerative disease that affects the CNS and results in motor disturbances [76], cell counts of motor neurons was deemed of greater importance so only the ventral horns have been analysed in this thesis. Motor neuron counts have been shown to decrease with time in mice with CLN1 NCL [4], so it was anticipated this may be true for CLN5 and CLN6 affected sheep too.

3.2 Sheep spinal cord area

At least five intact Nissl or GFAP-stained sheep spinal cord sections at each level (cervical, thoracic, and lumbar) for each animal at each age were photographed and analysed for area measurements. ImageJ software was used to manually draw around the total cross-sectional spinal cord area and the grey matter, in order to calculate the white matter using the equation:

White matter area = Total area – Grey matter area.

Little has been described in the literature about the healthy sheep spinal cord. Here, a qualitative comparison showed that it was relatively cylindrical or oval in shape, with greater width and depth (and hence area) in the cervical and lumbar regions than in the narrower thoracic region (Figure 3.1). Overall the cord was typically wider than it was deep and it reduced in depth but increased in width towards the caudal (lumbar) region. Between 3 and 18 months of age, the total cross-sectional and white matter areas from healthy control sheep (n=2-4 per age) increased (Figure 3.2, blue triangles), whilst grey matter volumes changed little over the same time period.

Even at 6 months of age, qualitative observation of the affected spinal cord showed a clear reduction in total cross-sectional area compared to the healthy control (Figure 3.2), however one-way ANOVA revealed no statistically significant differences between the genotypes in any region. There was a trend towards increased growth in the total area of the affected spinal cord between 3 and 15 months of age, before declining or plateauing at 18 months of age (Figure 3.2). The smallest cross-sectional areas were seen in the CLN5 affected spinal cord at every age assessed, but by end-stage disease (18 months) area measurements in the cervical and lumbar regions were comparable between the CLN5 and CLN6 disease models and these were noticeably smaller than the healthy control.

The total area measurements did not provide information on where the loss was occurring. Therefore, area measurements in the grey and white matter allowed for a more in-depth comparison. This revealed that, like the control spinal cord, there was very little reduction in the grey matter area and most loss occurred in the white matter. However, again this trend was not statistically significant.

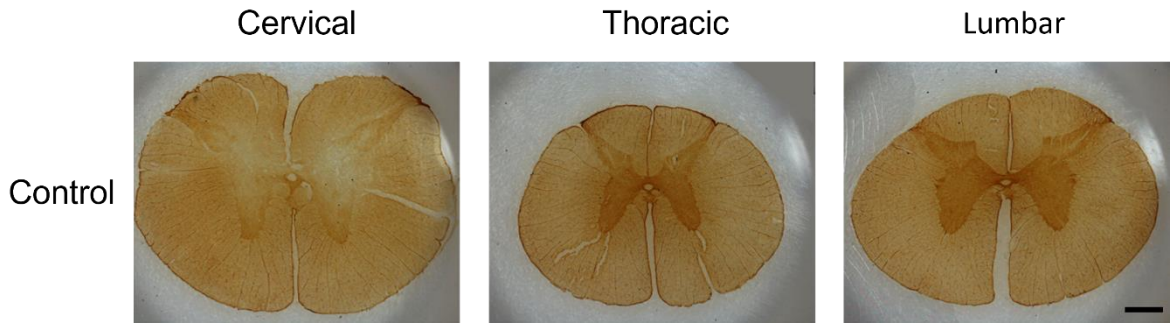


Figure 3.1 Regional differences in the healthy sheep spinal cord
 Representative spinal cord sections from a 6-month-old healthy control sheep. The scalebar represents 0.1 cm.

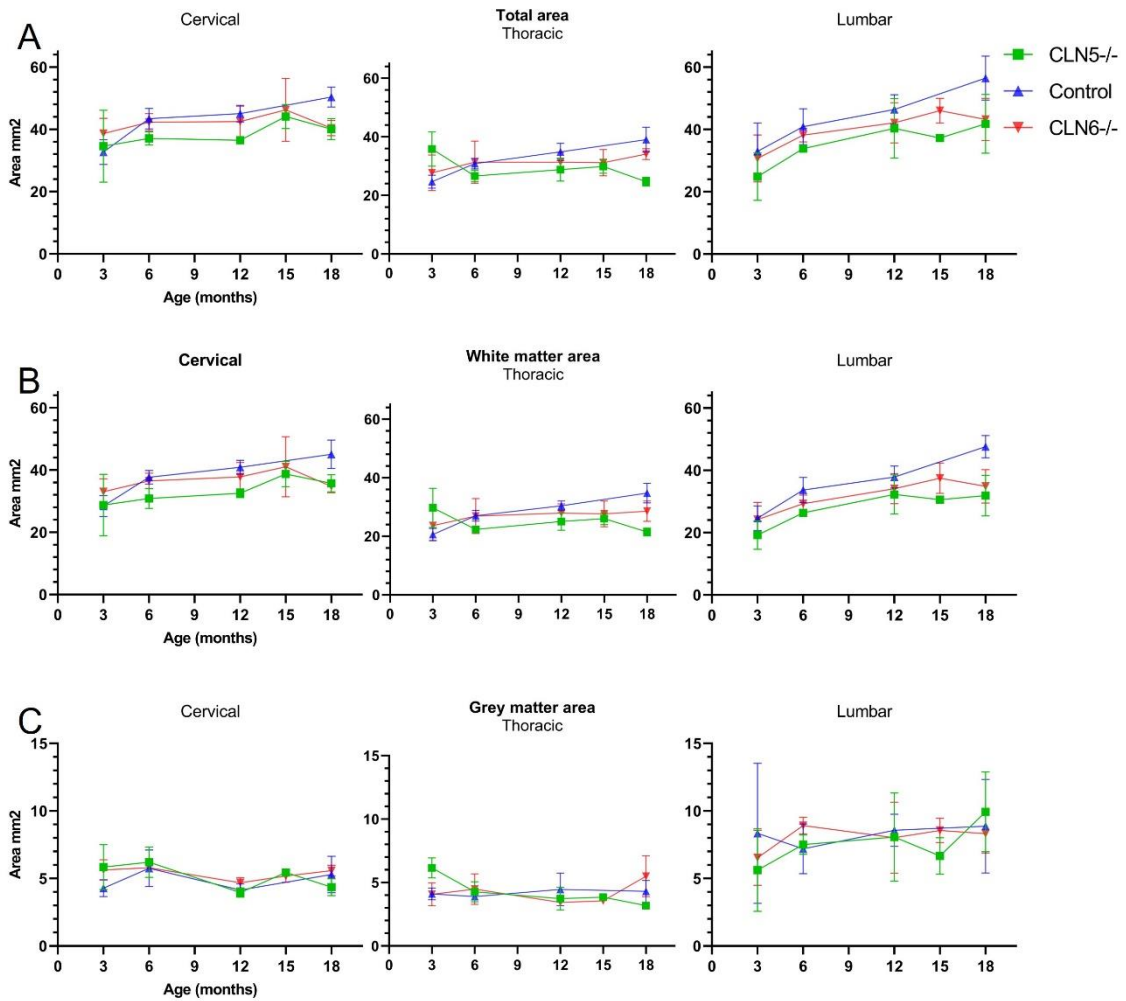


Figure 3.2 Comparative spinal cord areas during ovine NCL disease progression
 Quantification of the A. total cross-sectional area, B. white matter area and C. grey matter area of the sheep spinal cord. Area measurements (\pm SD) for $n = 2-4$ at each timepoint.

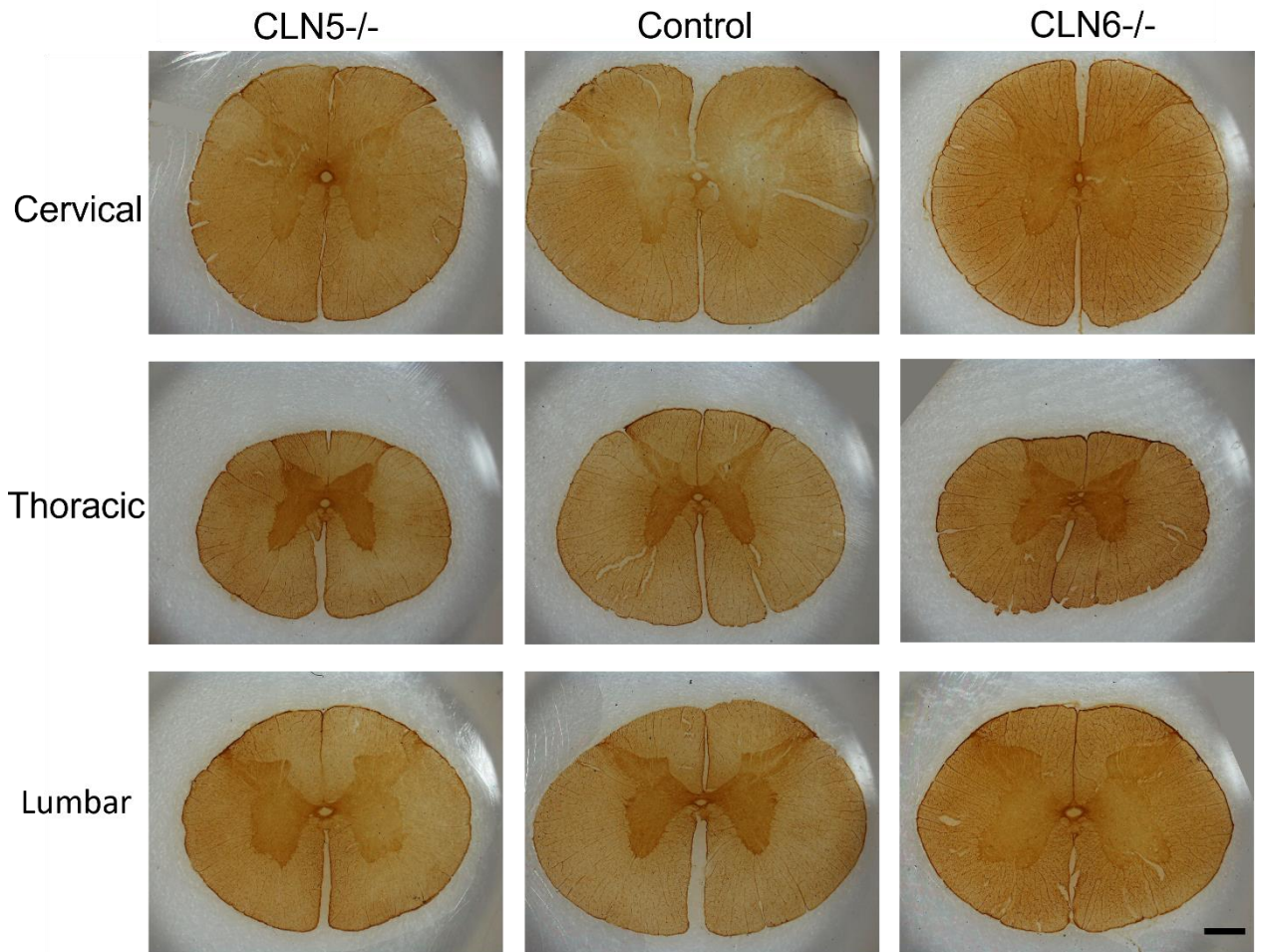


Figure 3.3 Regional differences between all genotypes in sheep spinal cord
 Representative spinal cord sections of all genotypes at 6-month-old. The scalebar represents 0.1 cm.

3.3 Neuronal loss in the ovine NCL spinal cord

The neuronal marker, NeuN, worked very well on thick (50 μ m) sheep brain sections. The NeuN sections were stained very precisely, revealing minimal staining in the white matter and very light neuropil staining, in combination with large darkly stained NeuN-positive cells.

In the ventral horn, it clearly stained the cell bodies and dendrites of the large motor neurons (Figure 3.4, red arrows). The cells were multipolar, often with an obvious nucleus, although the morphologies varied from fusiform, elongated, pyramidal, to polygonal, some with distinct processes. In the dorsal horn, NeuN- positive cells were typically smaller sensory neurons with minimal background (non-specific) staining and they had less obvious dendritic trees. Thus, it could be concluded that NeuN- immunoreactivity in the sheep spinal cord was specific to neuronal cell bodies, with very little neuropil in both horns.

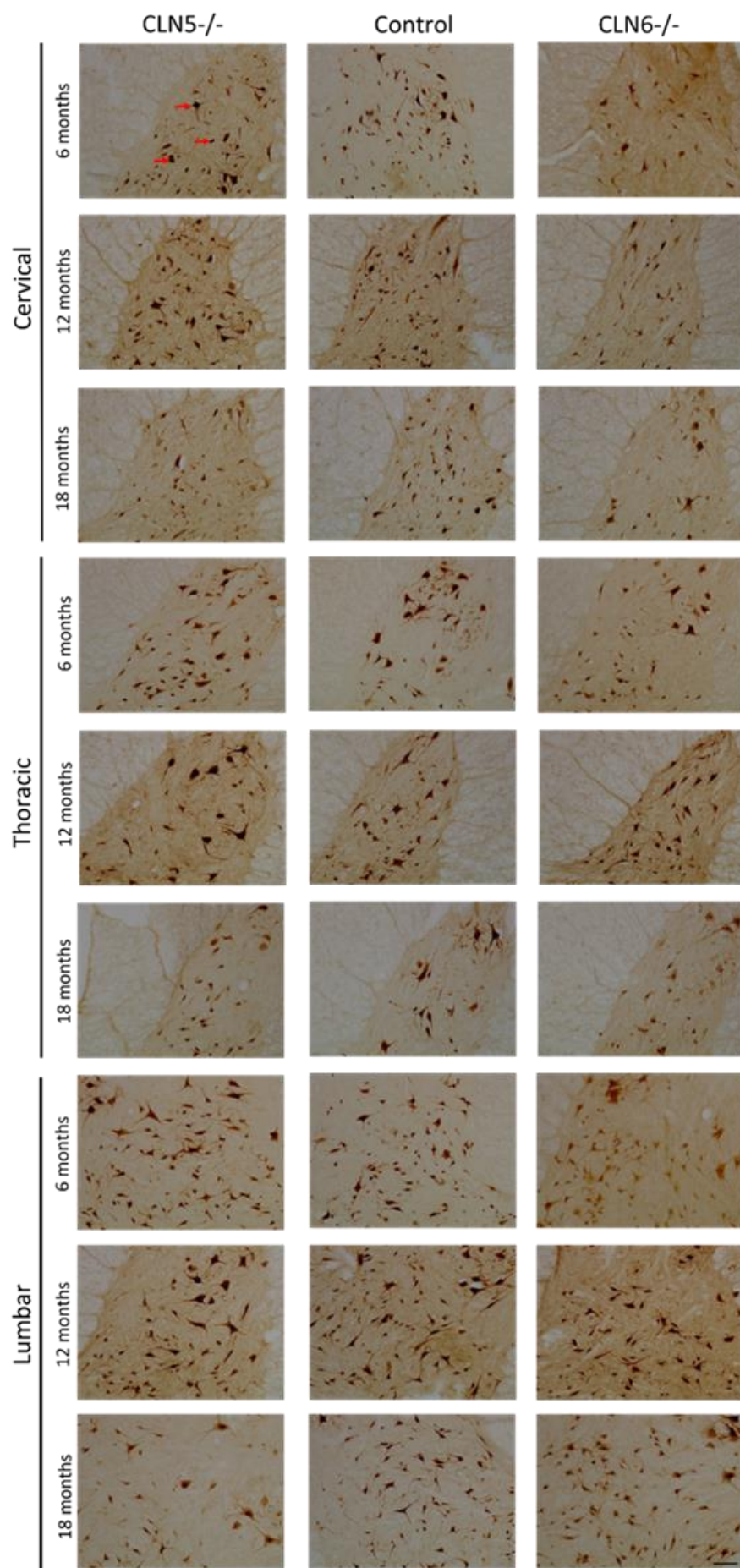


Figure 3.4 Representative images of NeuN-positive motor neurons in the ventral horn

Representative images of motor neurons of the ventral horn (red arrows) in the cervical, thoracic and lumbar spinal cord of control and CLN5 and CLN6 affected sheep at 6, 12 and 18 months of age. Sections were 50 μm thick. These demonstrated the diminishing concentration of motor neurons in CLN5^{-/-} animals compared to control sheep. The scale bar represents 100 μm .

When qualitatively comparing NeuN-positive cells in the ventral horn across the three spinal regions at 6, 12 and 18 months of age, there appeared to be some reduction in the number of large motor neurons in the CLN5 and CLN6 affected spinal cord over time (Figure 3.5). However, visual comparisons were made difficult by the variable size and shape of the NeuN-positive cell bodies and axon length. Automated neuronal counts of the larger motor neurons (diameter threshold $\geq 30 \mu\text{m}$) were performed (Figure 3.5). Control cell counts were relatively steady over time, with the most neurons detected in the lumbar region. Whilst one-way ANOVA failed to detect any significant differences between the genotypes, there was a general trend towards a reduction in NeuN-positive neurons in the ventral horn of all three spinal regions in CLN5 affected sheep (Figure 3.5). In particular, cell counts in the CLN5 affected cervical, thoracic and lumbar spinal cord halved between 6 and 18 months of age. However, most of this reduction in the two rostral regions occurred late in the disease course, between 12 and 18 months of age, at a time when motor deficits begin to manifest in CLN5 affected sheep [35]. In comparison, CLN6 affected motor neuron counts were similar to control numbers across the disease course, yet motor dysfunction has also been reported for ovine CLN6 disease [35].

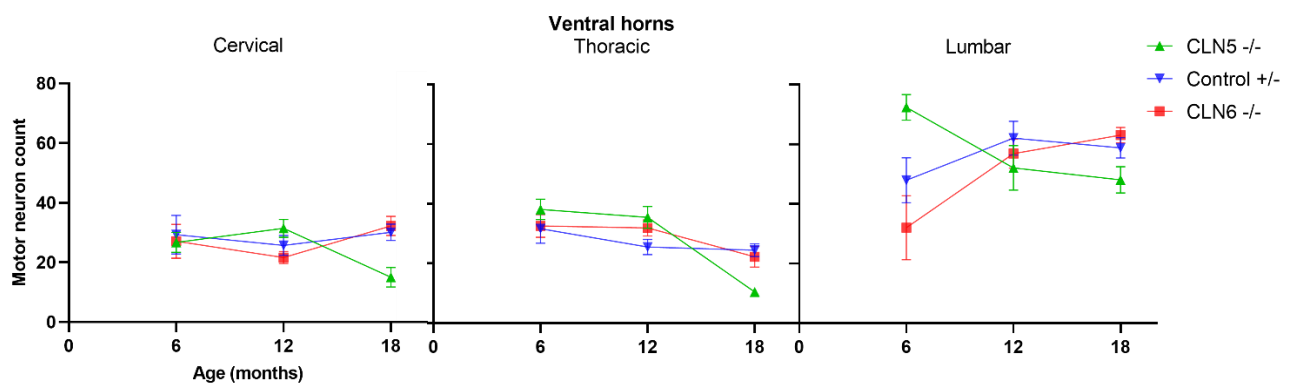


Figure 3.5 Motor neuron counts in the ventral horn during ovine NCL disease progression
Motor neuron counts (\pm SD) for n= 2-4 at each timepoint.

3.4 Lysosomal storage

Fluorescent lysosomal storage body accumulation is a key pathological hallmark of NCL. Progressive accumulation has been well documented in the affected sheep brain over the disease course [34, 35], so it likely accumulates in the spinal cord too. Fluorescent microscopy and image analysis of 50 μm thick spinal cord sections confirmed this. Whilst there were no disease-associated fluorescent aggregates in the healthy control sheep spinal cord, storage burden progressively increased in both the CLN5 and CLN6 sheep models (Figures 3.6 and 3.7). However, this increase only reached statistical significance by one-way ANOVA in the ventral horn of the lumbar spine ($p = 0.0422$) yet subsequent multiple t-tests failed to detect a significant difference between the genotypes at a single timepoint in this region. The punctate aggregates were largely confined to cells with characteristic neuronal morphology, including motor and sensory neurons.

A qualitative comparison across the disease course revealed two further important points (Figure 3.6). Firstly, higher levels of fluorescence were observed in the larger motor neurons of the ventral horn than in the smaller sensory neurons of the dorsal horn. This observation was true for both disease models.

Secondly, greater levels of fluorescent storage were present in the CLN6 affected spinal cord, than in the CLN5 affected spinal cord in all regions across the disease course (Figure 3.7). Accumulation in the CLN6 sheep model followed a near-linear increase from 3 months of age to reach levels as high as 3.5% in the lumbar ventral horn, whilst fluorescence levels in the CLN5 sheep model were largely steady between 3 and 15 months of age, before trending dramatically upwards at 18 months of age in all regions, except the cervical region.

There were unusual results at two time points – 12 months of age for CLN6 affected sheep and 15 months of age for CLN5 affected sheep. Large reductions in fluorescence were detected at these two timepoints, suggesting a possible error with sample collection or preparation.

Three and 18-month-old spinal cord samples from the same group of animals were also paraffin wax embedded and sectioned at 3 μm . This allowed for good visualisation of the fluorescent puncta within individual motor neurons and in non-neuronal cells (Figure 3.8).

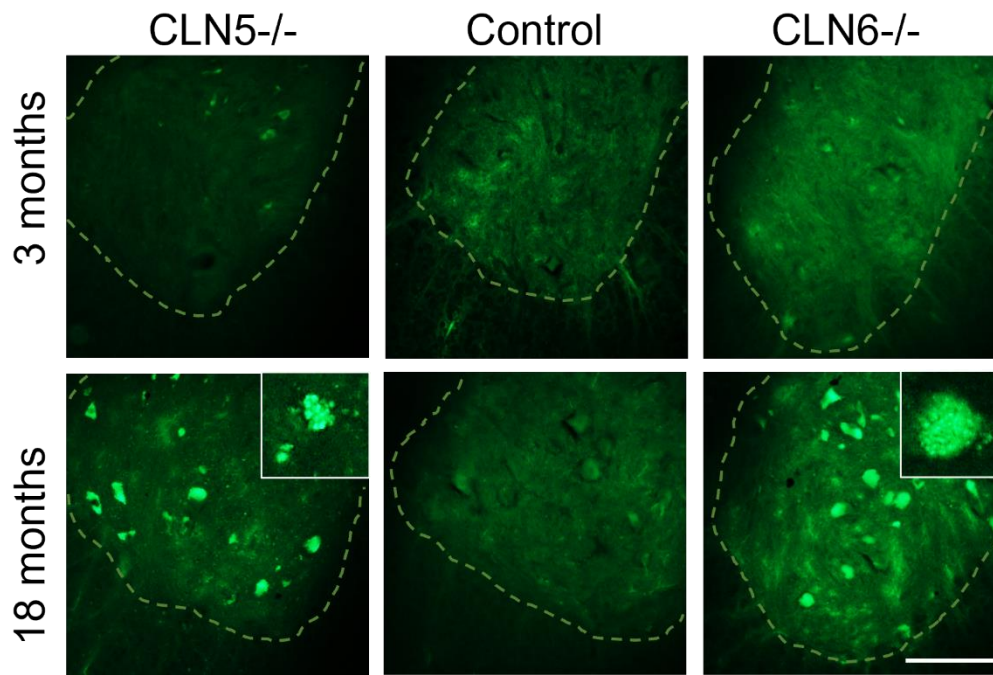


Figure 3.6 Fluorescent microscopy of 50 μm spinal cord sections

Representative fluorescent microscope images of the ventral horn of the lumbar spinal cord of control and CLN5 and CLN6 affected sheep at 3 and 18 months of age. These images revealed the obvious increase in lysosomal storage from 3 to 18 months of age in both CLN5 and CLN6 affected sheep, while there is no overt storage in the control sheep. The scale bar represents 200 μm and the dotted line indicates the grey and white matter boundary.

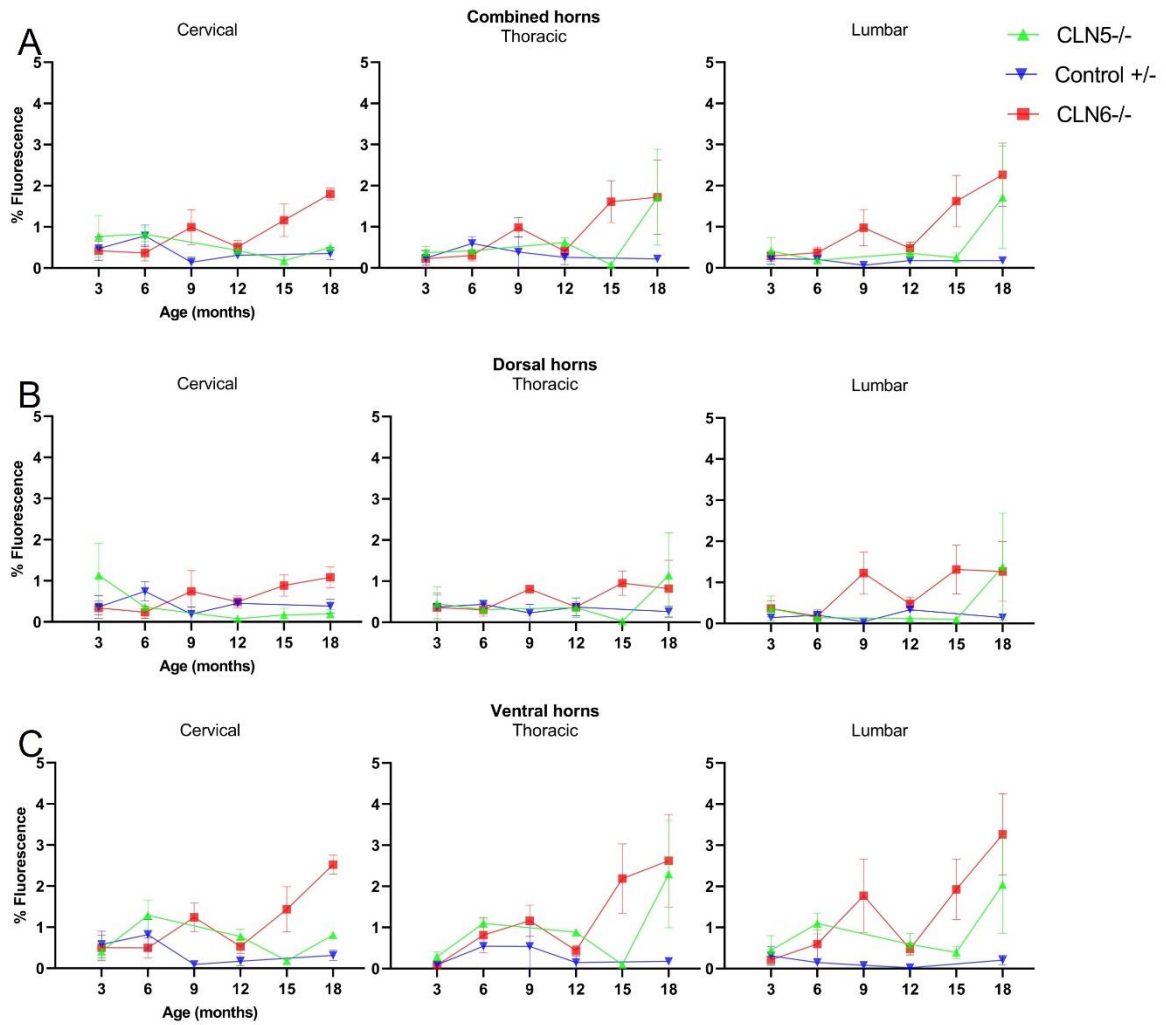


Figure 3.7 Accumulation of fluorescent storage bodies during ovine NCL disease progression
 Quantitative thresholding image analysis of fluorescence in A. the combined dorsal and ventral horns, B. the dorsal horns and C. the ventral horns. Percentage areas (\pm SEM) for n= 2-4 at each timepoint.

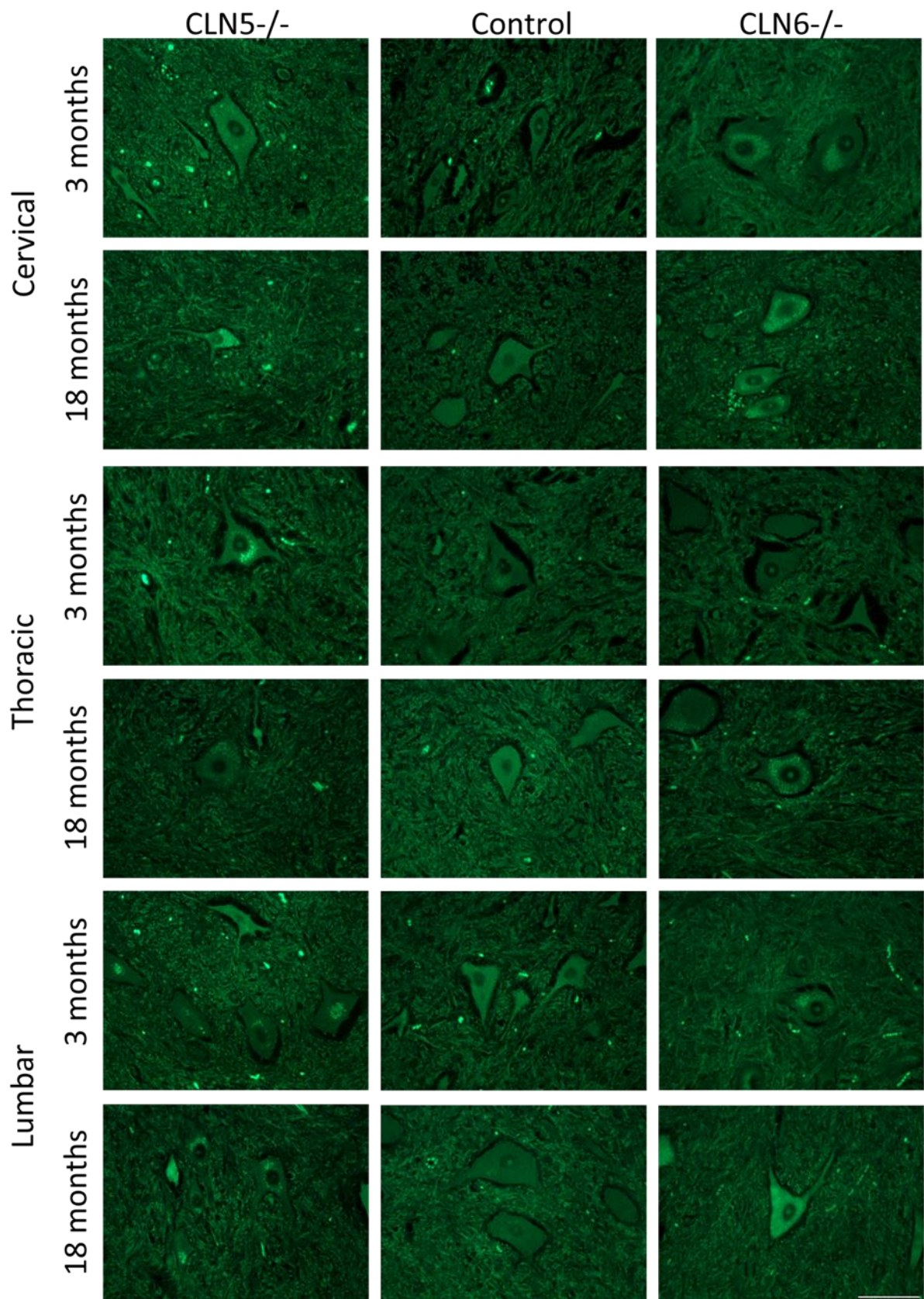


Figure 3.8 Fluorescent microscopy of 3 μ m spinal cord sections

Representative fluorescent microscope images of the ventral horn of the lumbar spinal cord of control and CLN5 and CLN6 affected sheep at 3 and 18 months of age. These images demonstrated fluorescent puncta located with the motor neurons and the progressive increase in affected sheep. The scale bar represents 50 μ m.

3.5 Discussion

This chapter explored key NCL pathology in the CLN5 and CLN6 affected sheep spinal cord. Neurodegeneration has long been studied in the brains of these affected sheep; it occurs regionally, with the most significant loss in the cerebral cortex while subcortical structures and cerebellum remain largely intact [34, 35, 71]. Lysosomal storage body accumulation occurs in the majority of cell types in the brains of affected humans [77, 78] mice [4, 68, 69, 79-81], and sheep [34, 35]. These key pathologies have also been described in the spinal cord of NCL mice and CLN6 affected Merino sheep [4, 18, 70], but this study is the first to explore them in the CLN5 Borderdale and CLN6 South Hampshire ovine NCL disease models.

3.5.1 Area measurements

Total cross-sectional area, as well as grey matter and white matter areas, were analysed across the disease course in healthy control, CLN5 and CLN6 affected sheep. Total area and white matter area in healthy control sheep grew over the time course, whilst they typically increased in CLN5 and CLN6 affected sheep from 3 to 12 or 15 months of age, before a trend towards reduction at late-stage disease (18 months of age) although this did not reach statistical significance. In contrast, the proportion of grey matter slightly reduced (CLN5 affected cervical and thoracic regions) or remained relatively constant (healthy control and CLN6 affected) over the disease course. This would suggest that the majority of the atrophy seen in affected sheep spinal cords at 18 months of age was coming from mild white matter atrophy. Similar studies of total, grey and white matter volumes in CLN1 affected mice at 1, 2, 3 and 7 months of age revealed there was little change in these volumes over the disease course, indicating that their spinal cords did not necessarily atrophy but rather did not grow in line with healthy control mice [18, 68]. It appears that in CLN5 and CLN6 affected sheep, spinal cord growth is not hindered until perhaps late-stage disease. Examination of volume measurements in further control and affected sheep, particularly at late-stage disease, may provide the necessary statistical power to confirm this.

A question remains on the accuracy of correlating NCL spinal cord findings in quadrupedal animal models, like mice and sheep, to the bipedal human condition. To date, there have been no studies which have investigated the possible differences between spinal degeneration in bipedal and quadrupedal models, or performed comparisons between sheep and human degenerative diseases. The only research has been limited to skeletal and physiological differences between the species [55]. It is known that ligaments, which maintain structure, and neuromuscular signalling develop differently in the quadrupeds and bipeds [82]. It is possible that innervation of the muscles and ligaments is different because of the orientation of the spinal cord, thus degeneration might be

observed in the regions of the spinal cord innervating the most affected muscles. However more research needs to be done to examine this further.

3.5.2 Neuron loss

Despite there being little change in the grey matter area over the disease course, neuronal cell counts were also performed to look for neurodegeneration in the spinal cord. This was achieved by staining with a neuronal marker, NeuN, which has proven to be a reliable tool for morphometric neuronal studies. For example, a comparison of Nissl and NeuN staining in the human cerebral cortex revealed that NeuN provided more accurate estimates of neuronal density and size, and stained a more circular perikaryal shape [83].

The ventral horn is primarily comprised of motor neurons, which are essential for controlling movement through their efferent projections to skeletal muscles. Because of the differences in cell populations residing in the dorsal and ventral horns, only the ventral horn underwent analysis to determine motor neuron number. This was investigated because loss of motor neurons in the spinal cord has been observed in other models of NCL, particularly the CLN1 mouse [4]. The thresholding size of motor neurons was chosen based on a previous study by Pamphlet et al who reported a motor neuron cell body diameter of approximately 30 μm in humans [84]. This threshold diameter was tested on some representative sheep spinal cord sections and found to detect the majority of large motor neurons. Subsequent counts revealed little change in control and CLN6 affected motor neuron numbers over time, but a clear loss of these large cells in the ventral horns of CLN5 affected sheep between 12 and 18 months of age.

These findings were interesting considering the onset and progression of motor dysfunction in CLN5 and CLN6 affected sheep is remarkably similar [35]. Both NCL sheep models exhibit early motor abnormalities, such as stumbling from 6 months of age, which progresses to more severe motor dysfunction with exaggerated gait, dyskinesia and then akinesia. However, it should be noted that severe motor dysfunction is a late-stage symptom of ovine NCL which typically occurs from 18 months of age, and observation of hundreds of sheep has failed to detect a faster clinical motor phenotype in CLN5 affected sheep than CLN6 affected sheep. Nevertheless, atrophic changes in the motor cortex do occur slightly earlier in the CLN5 affected disease model [35] so it is possible that this correlates with the earlier motor neuron loss in CLN5 affected sheep spinal cord seen in the current study.

Similar neuronal cell counts have been performed in the dorsal and ventral horns of CLN1 affected mice [80]. These revealed that there was significant loss of neurons at all three spinal cord levels as

early as 3 months of age [80], which was much earlier than neuronal loss in the brain [69, 80]. Unlike mice, it appears that neuronal loss in the CLN5 affected sheep spinal cord is a late-stage disease phenomenon, which occurs well after neuronal loss has occurred in the brain.

One concern with the neuronal counts was ensuring that the image collection was consistent. There were some discrepancies between the horn shapes, even within the same spinal cord regions, which may have impacted on neuronal cell counts. However, it was pleasing to see that the qualitative data matched the quantitative data. Going forward, cell counts could be attempted in the dorsal horn too, or alternatively threshold image analysis as used for other cell markers in this thesis (e.g. lysosomal storage, GFAP) could be used to determine the total area of NeuN-immunopositivity in both horns. This would ensure all neurons were counted, even those shrinking or dying, and not just those above the ≥ 30 μm diameter threshold.

3.5.3 Lysosomal storage

Lysosomal storage accumulation is documented to occur in numerous cell types [34], and increases linearly in the affected NCL sheep brain [34, 35]. The current study found that lysosomal storage also accumulated in the affected sheep spinal cord over time, with greater levels of fluorescent storage material in CLN6 affected sheep than CLN5 affected sheep. The CLN6 sheep model presented a near linear pattern of accumulation from 3 and 18 months whilst there was very little lysosomal storage accumulation in the CLN5 affected sheep spinal cord over the disease course, until a dramatic increase at 18 months of age. However, there was quite a bit of inter-individual variation (indicated by the large error bars) and statistical tests failed to detect a significant difference between the genotypes at any age.

The CLN6 spinal cord data correlates well with published literature on lysosomal storage accumulation in the affected sheep brain [34, 35] as it also follows a near linear pattern. However, storage is seen as early as birth in the brain, with significant differences in fluorescence levels between the healthy control and CLN5 and CLN6 affected sheep across all regions of the brain, except the white matter, by 6 months of age [35]. It appears that the lysosomal storage in the spinal cord increases at a slower rate, as there was no obvious difference between the healthy control and affected sheep samples until 15 to 18 months of age.

Microscopically, it was observed that there was a greater intensification of fluorescence in the larger motor neurons in the ventral horn compared to the small sensory neurons located in the dorsal horn. This result is not necessarily surprising. The ventral horns have a larger carrying capacity because of the size of their motor neurons compared to the smaller sensory neurons in the dorsal horn. A similar result is observed in the affected sheep cerebellum, where the large Purkinje neurons

accumulate large quantities of lysosomal storage whilst the much smaller cerebellar granule cells only have modest levels of storage (Nadia Mitchell, personal communication).

3.5.4 Trouble-shooting

A discrepancy in sampling was noticed throughout this study, particularly while carrying out the area measurements. It became clear that there were overt differences with the size and shape of the sections harvested. This was especially so in the cervical region, as well as some lumbar spine sections. The width and depth of the sheep spinal canal varies along the length of the spinal cord however it maintains a similar pattern to the human spinal cord. The canal at the level of the cervical vertebrae in both species is at its narrowest at cervical level C2, whilst C7 is wider and deeper (Figure 3.9) [55]. This would indicate that the precise location of sample collection needs to be consistent, otherwise subsequent area comparisons between animals could be flawed. For the current study, thoracic samples were consistently collected from the T7-T9 region and lumbar samples from L2-L4 but cervical samples were collected from either the C2-C3 or C5-C7, depending on the method of euthanasia.

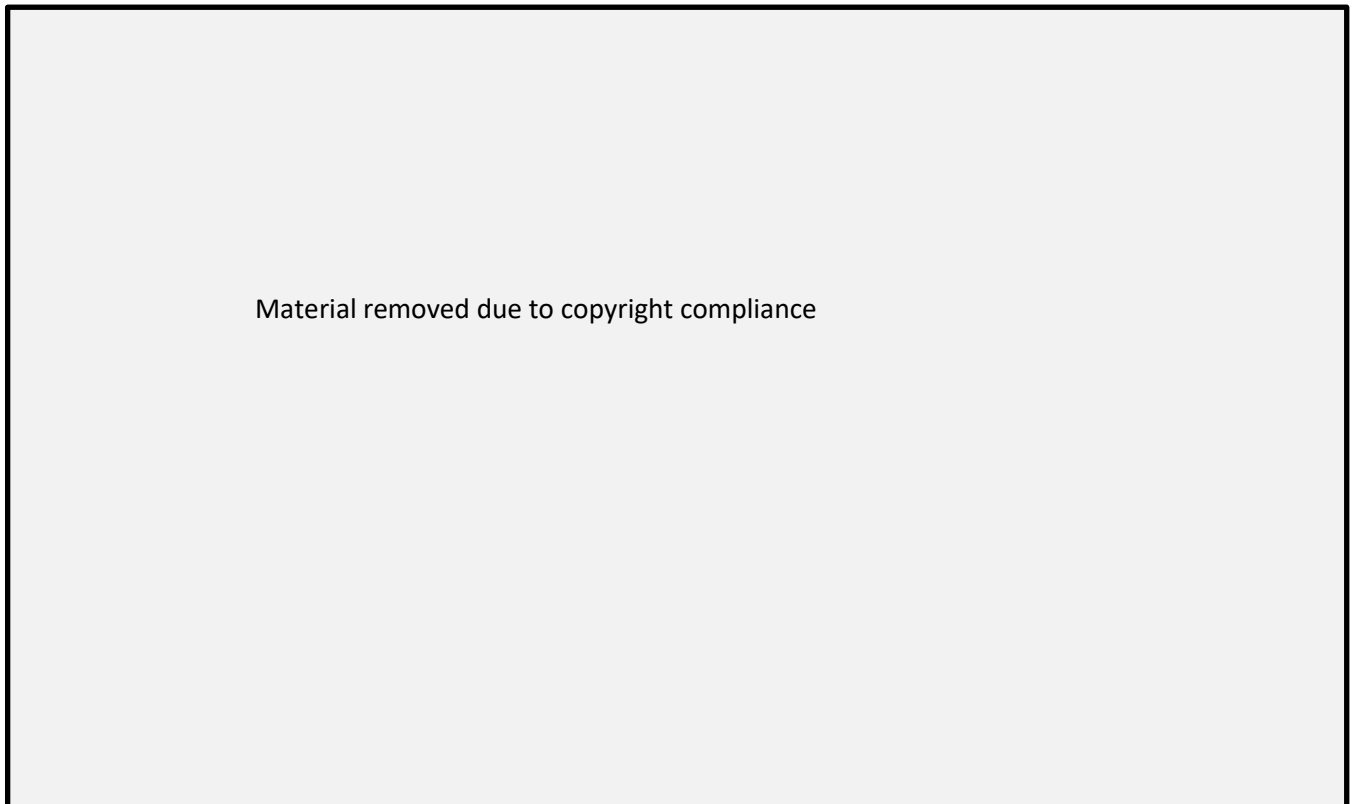


Figure 3.9 Variation of the spinal cord width and depth for sheep and human

Representation of the spinal canal width (red) and depth (blue) was compared along the length of the spine and across many studies in sheep (filled symbols) and humans (open symbols). The varying symbols represent a published study. Figure modified from Wilke et al [55].

Secondly, on interpretation of the lysosomal storage data, it became clear that there were two timepoints which went against the trend. These were at 12 months of age in CLN6 affected cords and 15 months of age in CLN5 affected cords. At each of these timepoints, the percentage area of fluorescence fell compared to the data collected at adjacent ages. It is possible that this was due to a delay between sectioning these samples and mounting for fluorescent analysis, as sections for these two timepoints were not imaged until all individuals in their group were sectioned. Communication with a leading NCL pathologist has revealed that lysosomal storage can be quenched in CNS tissue (Jon Cooper, personal communication) and moving forward it will be vital to section, prepare and image all spinal cord samples through the disease course at the same time.

Finally, even though many of the current results did not reach statistical significance, there were clear trends, and data from more individuals may improve statistical power to further confirm the findings. In particular, three animals of each genotype will be euthanised in February 2023 and spinal cord samples will be collected. This will increase the number of animals to be analysed at this late-stage disease timepoint to n=5 per genotype.

3.5.5 Conclusion

- Total area and white matter area increased in CLN5 and CLN6 affected sheep spinal cords from 3 to 15 months, prior to a dramatic reduction in area at 18 months. The grey matter showed a mild loss or stayed consistent. Neuron counts in the ventral horn of CLN6 affected sheep remained similar to control sheep, while there was a reduction in numbers in the CLN5 affected thoracic and lumbar spine regions between 12 and 18 months.
- Lysosomal storage was higher in the CLN6 affected sheep spinal cord compared to the CLN5 affected sheep. Interestingly, the CLN5 fluorescence remained steady until a dramatic increase at 18 months of age (end-stage disease), while the CLN6 level just increased linearly.
- A difference between spinal degeneration in bipedal and quadrupedal species is possible, however this is currently unstudied.

Chapter 4

Neuroinflammation in the NCL spinal cord

4.1 Introduction

Neuroinflammation is a common pathological hallmark of NCL in the brain, but it has also been documented to increase with disease progression in the spinal cord in a mouse model of CLN1 NCL [4, 18, 68] (Figure 4.1). These studies used immunohistochemistry or immunofluorescence with a common astrocytic marker (GFAP, glial fibrillary acidic protein) and microglial marker (CD68) to show a progressive neuroinflammatory response in the dorsal and ventral horns of the affected mouse spinal cord grey matter.

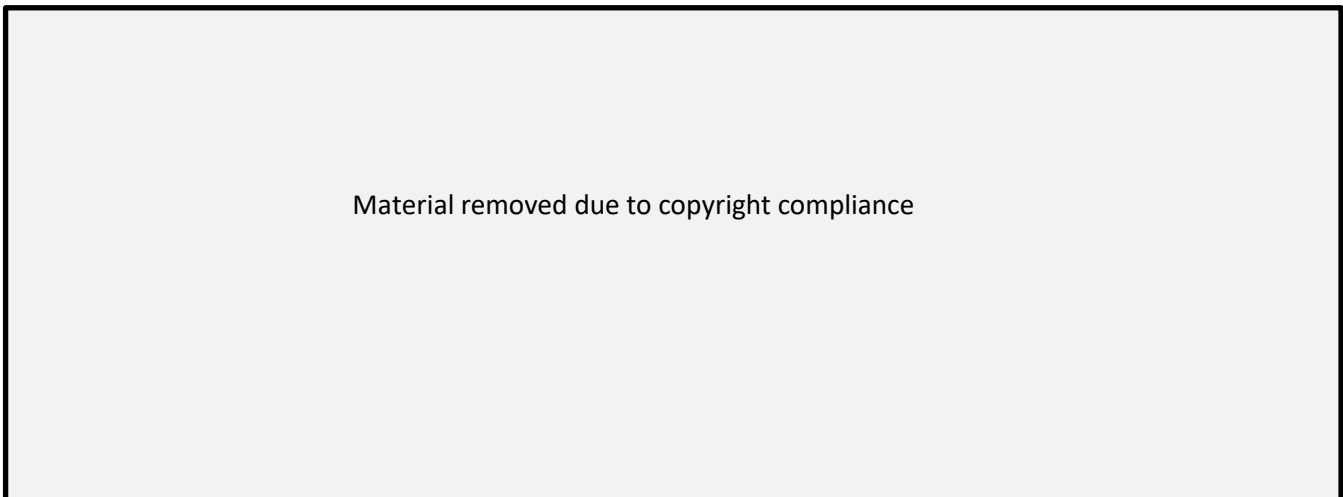


Figure 4.1 Early glial activation in CLN1 affected mouse spinal cords

Representative images of progressive astrocytosis (GFAP immunoreactivity) and microgliosis (CD68 immunoreactivity) in CLN1 affected (*Ppt1*^{-/-}) mice. Modified from Nelvagal et al., 2021 [68].

This chapter presents a detailed study of astroglial pathology in the ovine CLN5 and CLN6 disease models. However, to understand neuroinflammation in the spinal cord, it is first necessary to understand the location and morphologies of its astroglial populations. Astrocytes are believed to be the most numerous cell in the vertebrate central nervous system, however a complete understanding of their function is unknown [85]. It is known that astrocytes are supportive cells, regulating and maintaining endothelial cells at the blood brain barrier, and are involved in homeostasis, as well as providing nutrients [85]. They are also essential for expediting axonal myelination, however, their role in this process is still unclear [86]. Astrocytes are located both in the grey and white matter in the CNS, although there are particular regions where they are found at significantly higher concentrations, in particular under the dura and around cerebral vasculature [86]. The presence of activated astrocytes has been noted in the brains of sheep with CLN5 and CLN6 NCL

and they represent a precursor for subsequent neurodegeneration [32, 34, 35]. In CLN1 affected mice, activated astrocytes were predominantly located in the grey matter of the spinal cord but were also present in the white matter [4].

Distinctive astroglial morphologies are seen between the grey and white matter [87]. Astrocytes in the white matter have smaller cell bodies, with processes which align with myelinated fibres, and are termed fibrous [86]. Grey matter astrocytes are protoplasmic in appearance, being larger, sheath-like and they have more processes or branches [86]. However, when activated their morphology changes as the size of their cell body increases and their branches both shorten and thicken. If the activation remains for an extended period of time, inflammatory oxidative and nitrosative stress can be exacerbated which is deleterious for neurodegenerative diseases [44]. Figure 4.2 [88] nicely demonstrates the healthy and pathological morphologies of white matter astrocytes in the mouse spinal cord.

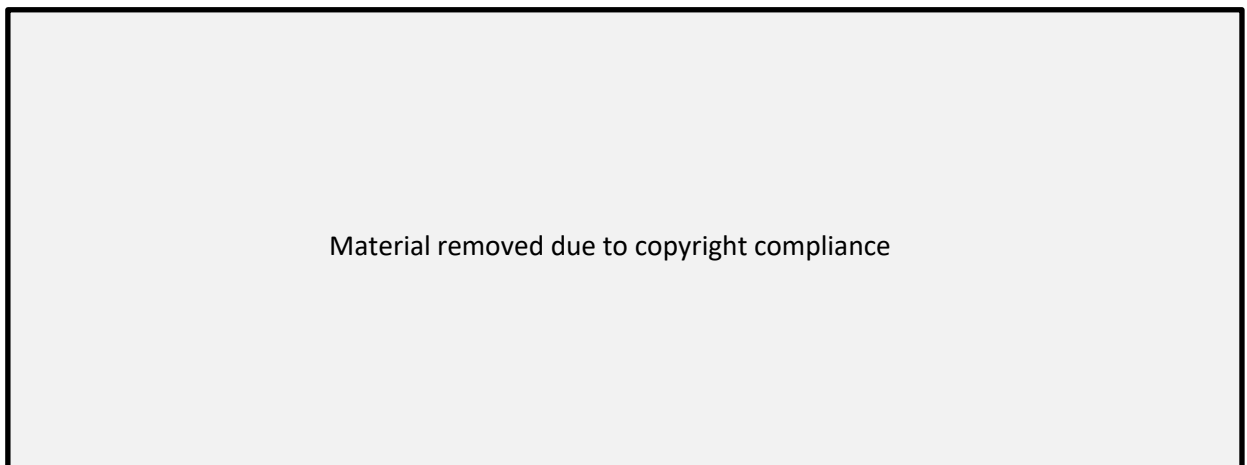


Figure 4.2 GFAP-immunostained sections of white matter of the spinal cord in mice
A. Healthy fibrous white matter astrocytes form part of the lattice pattern around myelinated axons (white circles with internal blue stained axons). B. Reactive astrocytosis in the white matter. Note the greater quantity of activated astrocytes with shorter thickened cytoskeletal processes [88]

As progressive astrocytosis has been documented to occur in sheep with CLN5 and CLN6 disease and the spinal cord is simply an extension of the central nervous system, it was anticipated that glial activation would also occur in their spinal cord. Activation was assessed by immunohistochemistry and immunofluorescence using the astrocytic marker GFAP on both thick (50 μm) and thin (3 μm) spinal cord sections from healthy control, CLN5 and CLN6 affected sheep.

4.2 Materials and Methods

A dilution series was first performed using the immunohistochemical GFAP staining method described in Section 2.6.2, and GFAP immunofluorescence was also attempted. These additional methods are described below.

4.2.1 GFAP immunohistochemistry dilution series of thick 50 µm spinal cord sections

An initial dilution series of the rabbit anti-cow GFAP antibody (Z0334, Dako, Ely, England) was attempted on 15-month-old CLN6 affected and control 50 µm spinal cord sections using the method described in Section 2.6.2. It included 1:5,000, 1:6,000, 1:6,500, 1:7,000, 1:7,500, 1:10,000, 1:15,000, and 1:20,000. This determined 1:10,000 to be the optimal dilution, hence this concentration was used for subsequent immunohistochemical GFAP studies on thick 50 µm spinal cord sections.

4.2.2 GFAP Immunohistochemistry on thin 3 µm spinal cord sections

Formalin fixed spinal cord tissues (cervical, thoracic and lumbar) from 3 and 18-month-old CLN5 affected (*CLN5^{-/-}*), CLN6 affected (*CLN6^{-/-}*) and healthy control sheep were paraffin embedded, sectioned at 3 µm and mounted on glass slides by Gribbles Veterinary Pathology (Christchurch, New Zealand). Slides were then dewaxed twice in xylene, 10 min each, rehydrated in ethanol and then blocked in 3% H₂O₂ in methanol, 20 min. A hydrophobic pen was used to draw around the section, before incubation in 400 µl blocking agent (25% normal goat serum (NGS, Invitrogen, Carlsbad, CA, USA) in Tris Buffered saline with 0.1% Tween X-100 (TBST)), 30 min at room temperature. Sections were incubated in the primary antibody (GFAP, 1:1,750, Z0334, Dako) in 10% NGS in TBST overnight at 4°C, followed by a goat anti-rabbit IgG biotinylated secondary antibody (1:500, B7389, Sigma-Aldrich, Australia), 30 min at room temperature. After a 30 min incubation in Extravidin – Peroxidase conjugate (1:1000, E2886, Sigma-Aldrich) in PBS, immunoreactivity was detected with 0.5 mg/ml diaminobenzidine tetrahydrochloride (DAB, D5637, Sigma-Aldrich) containing 0.01% H₂O₂ in PBS, 7 min. Slides were rehydrated, placed in xylene twice, 5 min, and coverslipped using DPX (BDH, Poole, England).

4.2.3 GFAP immunofluorescence on thick 50 µm spinal cord sections

GFAP immunofluorescence was performed on all three genotypes at one timepoint (12 months of age), using a similar method to that described in Section 2.6.2. After incubation in the primary GFAP antibody (1:1,750), 60 h at 4°C, sections were incubated in an Alexa Fluor 594 Goat anti-Rabbit IgG secondary antibody (1:1000, A-11012, Thermo Fisher Scientific, Waltham, MA, USA), 24 h, at room

temperature in the dark. The slides were then mounted, and cover slipped with anti-fade fluorescence mounting medium (ab104135, Abcam, Cambridge, UK) and immunofluorescence examined on the Nikon Eclipse 50i microscope (Nikon Instruments Inc., Tokyo, Japan), utilising NIS-Elements software (v. 4.50, Nikon Instruments).

4.3 Results

4.3.1 GFAP immunohistochemical dilution series

A dilution series is used to calculate the concentration best suited for a specific method. In this case, the GFAP antibody had been successfully used at 1:5000 on sheep brain sections [34], but was untested in the sheep spinal cord. Visual inspection of the samples led to the decision to proceed with a 1:10,000 dilution (Figure 4.3). This concentration was dark enough to see astrocytic staining in the grey matter, but provided light enough background for the visual distinction between the affected and control samples.

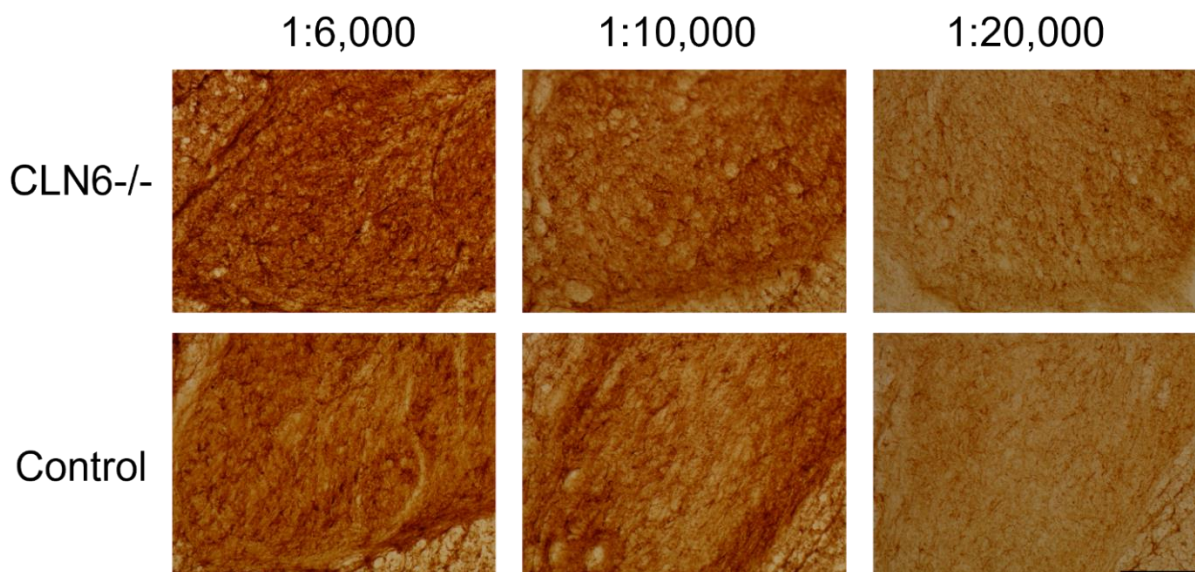


Figure 4.3 GFAP dilution series

GFAP immunostaining was compared in the lumbar dorsal horn of 15 month affected (*CLN6^{-/-}*) and 18-month control 50 μ m sheep spinal cord sections at a range of antibody dilutions. Scale bar represents 100 μ m.

4.3.2 GFAP immunohistochemistry in thick 50 μ m spinal cord sections

Astrogliosis is widely associated with neuronal loss in the brain of CLN5 and CLN6 affected sheep, and it actually precedes neurodegeneration [34, 35]. GFAP immunostaining of cervical, thoracic and lumbar spinal cord samples revealed there was very little distinguishable difference in immunoreactivity in the grey matter between the healthy control, and CLN5 and CLN6 affected

sheep at either 3 or 18 months of age (Figures 4.4 and 4.5). In all three genotypes, there was a strong meshwork of protoplasmic GFAP-positive astrocytes in the grey matter which overlapped and made it difficult to see individual cells. The 18-month samples had less intense neuropil staining, allowing for better differentiation of cells and there appeared to be some potentially activated cells on the lateral periphery of the horns but this occurred in both control and diseased spinal cord samples. Interestingly, threshold analyses indicated a reduction in GFAP immunopositivity in all three groups between 3 and 18 months, which contrasted the astroglial upregulation reported in CLN1 affected mice [4]. Whilst statistical analysis by one-way ANOVA failed to detect any significant differences between the genotypes, this trend was apparent across the three spinal cord regions and also between the dorsal and ventral horns.

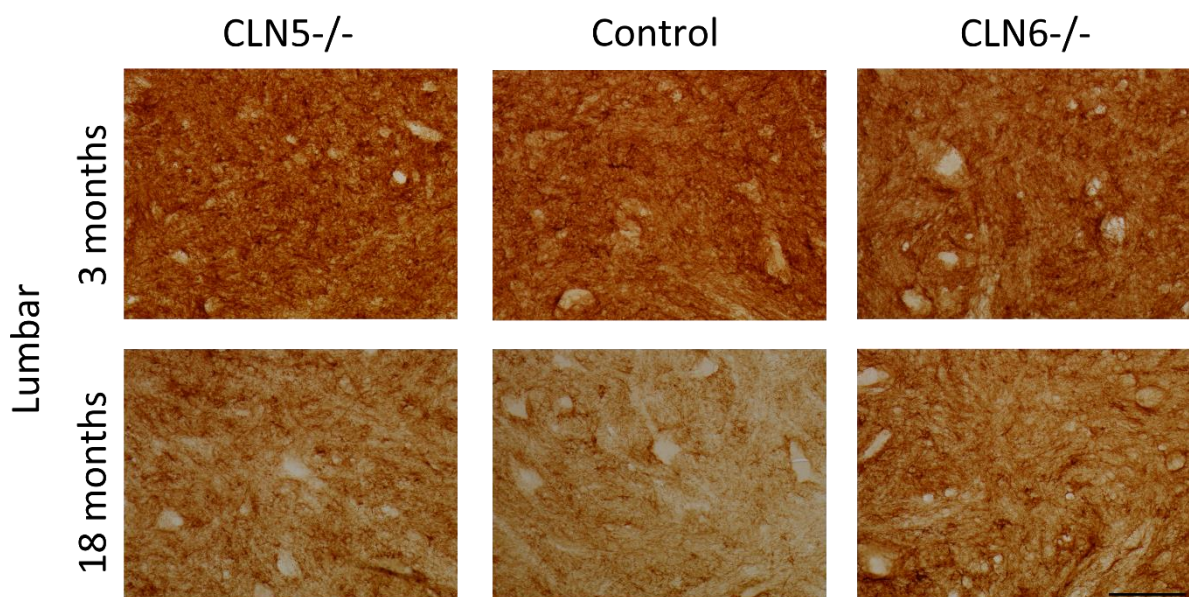


Figure 4.4 Astrocytosis in the spinal cord during ovine NCL disease progression
Representative images of GFAP staining in the ventral horn of the lumbar spinal cord of control, CLN5 and CLN6 affected sheep at 3 and 18 months of age. There was a reduction in immunostaining in all three groups between 3 and 18 months of age. Scale bar represents 100 μm .

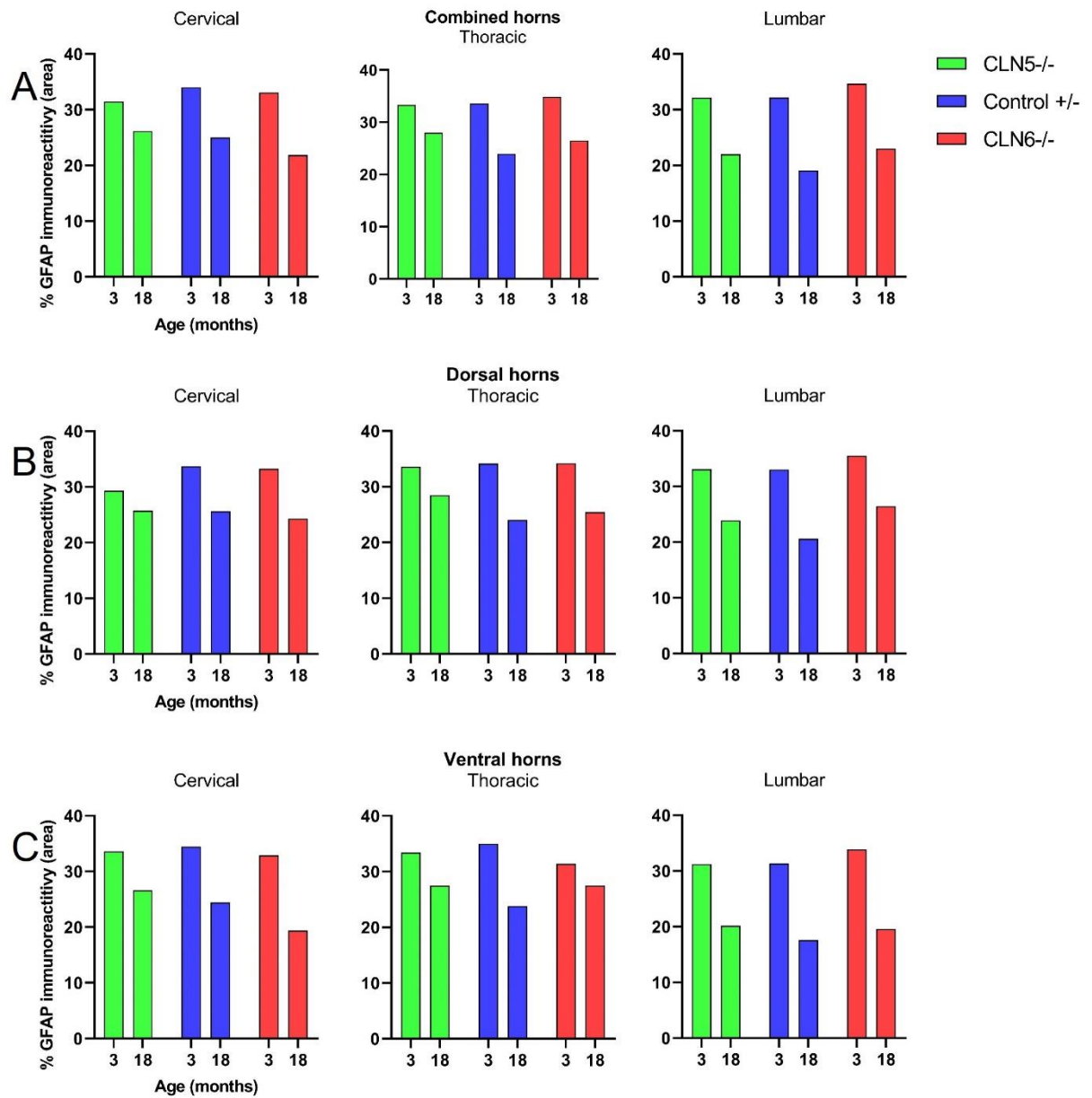


Figure 4.5 GFAP immunoreactivity during ovine NCL disease progression

Quantitative thresholding image analysis of GFAP immunostaining in A. the combined dorsal and ventral horns, B. the dorsal horns, and C. the ventral horns of the 50 μ m spinal cord.

4.3.3 GFAP immunohistochemistry in thin 3 μm spinal cord sections

As the GFAP result in the thick 50 μm spinal cord sections was unanticipated, glial activation was also assessed in thinner 3 μm sections. It was hoped that the thinner sections might provide a clearer image of GFAP expressing cells and allow for a morphological study to be carried out. Results presented are purely qualitative.

A comparison of the healthy sheep spinal cord at 3 and 18 months indicated little obvious change in the astroglial populations over time. Healthy protoplasmic astrocytes were evident throughout the dorsal and ventral horns (Figure 4.6), whilst fibrous astrocytes formed part of the white matter lattice (Figure 4.7). There was more neuropil staining at 3 months of age, and larger axons at 18 months of age, indicating axonal maturation and the development of mature myelination.

The CLN5 affected spinal cord also had darker neuropil staining at 3 months of age (Figure 4.6), suggesting it was a developmental phenomenon. There were potentially fewer GFAP-positive cells in the CLN5 affected grey matter at 18 months of age compared to the earlier timepoint but even late-stage disease, there was no obvious increase in activated cells and the CLN5 affected grey and white matter resembled the age-matched healthy control (Figure 4.6 and 4.7).

This contrasted with the CLN6 affected spinal cord, which had larger, more intensely stained cells in both the grey matter (Figure 4.6), and particularly the white matter (Figure 4.7) at 18 months of age. These white matter astrocytes still aligned with the myelinated fibres but their cell somata were increased in size and their branches had thickened, indicative of their activated morphology.

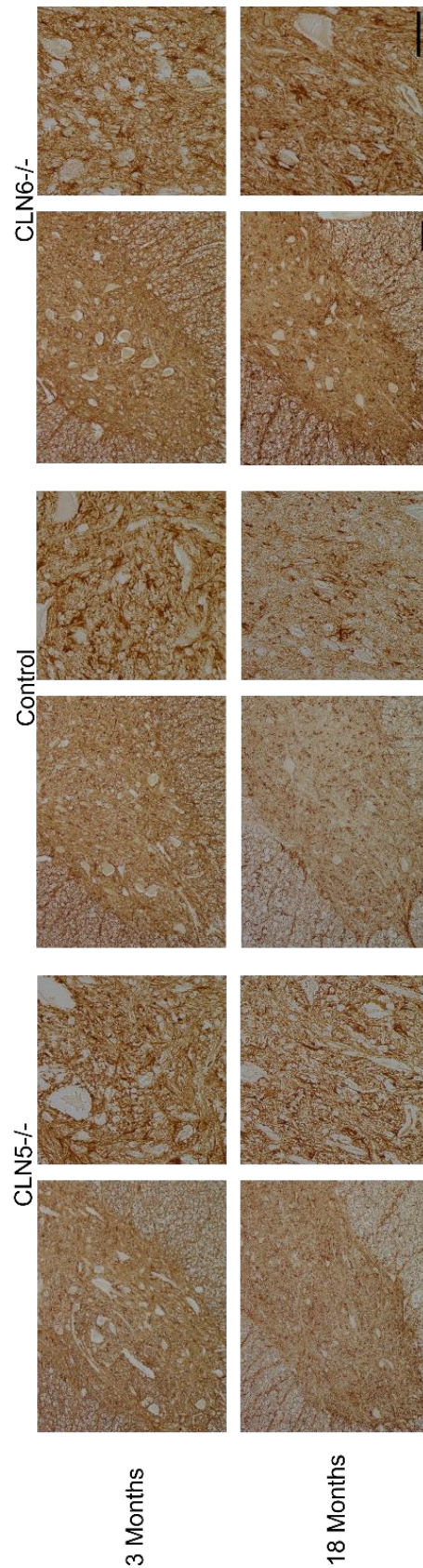


Figure 4.6 Astrocytosis in the spinal cord grey matter during ovine NCL disease progression
 Representative images of GFAP expression in the ventral horn of the thoracic spinal cord of healthy control, CLN5 (*CLN5*^{-/-}) and CLN6 affected (*CLN6*^{-/-}) sheep at 3 and 18 months. Images were taken on 3 μm sections at two magnifications, and the scale bar represents 100 μm and 50 μm for the rectangle and square images respectively.

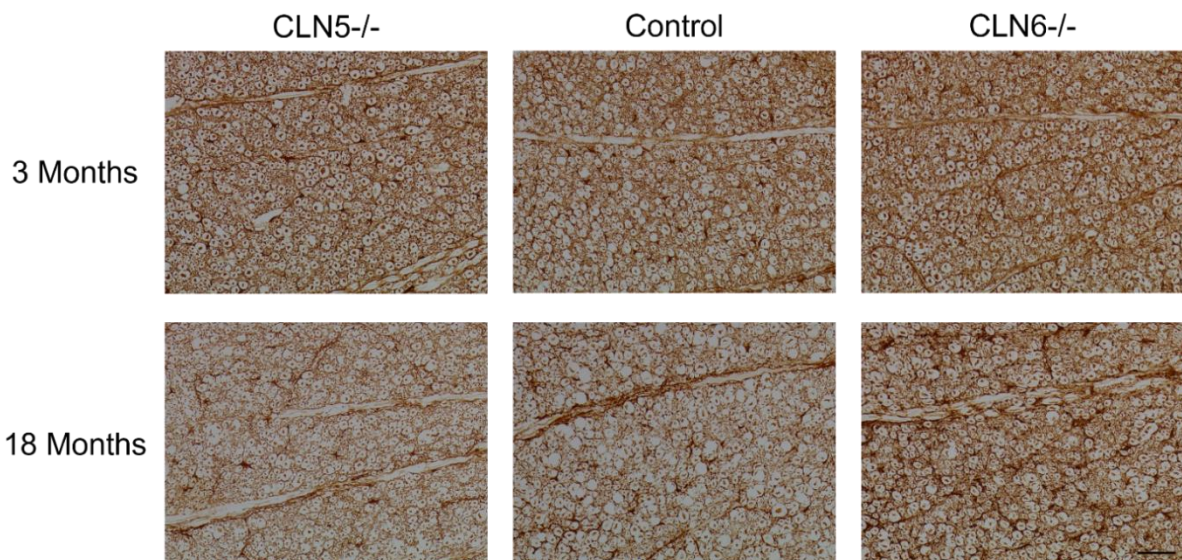


Figure 4.7 Astrocytosis in the spinal cord white matter during ovine NCL disease progression
 Representative images of GFAP expression in the white matter of the spinal cord of healthy control, CLN5 and CLN6 affected sheep at 3 and 18 months, cut at 3 μm . Note the increase in activated astrocytes in the CLN6 affected sheep spinal white matter at end-stage disease. The scalebar represents 100 μm .

4.3.4 GFAP immunofluorescence in thick 50 μm spinal cord sections

Immunofluorescence can provide greater sensitivity and signal amplification compared to the immunoperoxidase methods used above. However, the immunofluorescence technique did not provide a clearer image of glial activation in the sheep spinal cord. When slides were examined under the microscope, the fluorescent signal was ubiquitous, thus clearly not showing the glial activation seen in previous studies in CLN1 affected mice using the same method (Figure 4.1, [68]). Due to the ubiquity, it was not possible to see any increase in GFAP positivity in CLN5 and CLN6 affected sheep. Unfortunately, the slides were disposed of prior to imaging, thus not was not possible to provide an image of the result.

4.4 Discussion

4.4.1 GFAP immunohistochemistry in thick 50 μm spinal cord sections

GFAP immunostaining of 50 μm control and CLN5 and CLN6 affected spinal cord tissues at 3 and 18 months failed to detect any difference between the three genotypes. Although there is a non-significant reduction in GFAP immunoreactivity from 3 to 18 months, this occurred in both diseased and healthy control spinal cords and was the opposite to what has been observed in CLN1 affected mice. Early glial activation was documented to occur in all levels of the affected mice spinal cord [4, 68]. As early as 1 month of age, there were numerous GFAP positive astrocytes in the grey matter

but with no clear laminar pattern of staining [68], and by 5 months the entire grey matter was filled with highly active astrocytes [4].

The fact that CLN5 and CLN6 affected sheep spinal cords do not show upregulated astroglial activation was unanticipated, given it is an early observation in the brain of affected sheep [34, 35]. Reasons for this discrepancy were explored and a plausible explanation was that the 3- and 18-month sheep spinal cord samples were processed in different batches. Although the same experimental procedure was followed (Section 2.6.2) and the incubation time in DAB was identical (5 minutes), immunohistochemistry is well known for inter-batch variation [89]. In future studies of this type, all GFAP samples should be processed and undergo analyses together to remove this possibility. Alternatively, if the experiment involves too many samples for this to be possible, a consistent batch control must be used to regulate any differences.

4.4.2 GFAP immunohistochemistry in thin 3 μm spinal cord sections

GFAP immunohistochemistry was also carried out on 3 μm thin spinal cord sections as the results from the 50 μm sections were unanticipated. The thickness of the 50 μm section can cause a meshwork of overlapping cells, thus it was hoped that using thinner sections would resolve this to a single cell layer providing a clearer image. Due to the cost of external wax-embedding and sectioning at Gribbles Veterinary Pathology, only two timepoints were selected, being a 3-month-old pre-symptomatic age and 18-month-old end-stage disease. Additionally, only one region of the spinal cord sections were imaged as that region was the most intact after external processing. Unlike the 50 μm spinal cord staining, the 3- and 18-month-old thin sections were all run in one batch, therefore removing inter-batch variability.

Results presented from the 3 μm sections were purely qualitative, but surprisingly they paralleled those seen in the thicker sections. Visual observation revealed a comparable reduction GFAP expression in both the grey and white matter of control and CLN5 affected sheep between 3 and 18 months of age. However, there appeared to be an increase in GFAP-positive cells with activated morphology in both the grey and white matter of the CLN6 affected spinal cord at 18 months, compared to 3 months of age. This was especially apparent in the white matter where activated astrocytic cell bodies were distended with shortened, thickened branches compared to a healthy fibrous morphology. This seemed to more closely match the upregulation of astrocytosis seen in CLN1 affected mice grey and white matter, [4, 68], but just not to the same intensity.

As mentioned, these results were purely qualitative although there is no reason why they couldn't be quantified. Quantitative thresholding analysis could be used as has been employed for the thicker

sections detailed elsewhere in this thesis. The n number for these studies was two per genotype, thus there is potential to statistically improve the outcome by including the other two spinal cord regions (cervical and lumbar) in the analyses and increasing the n number per genotype. As detailed previously, spinal cord samples from three additional animals of each genotype will be collected in February 2023 at 18 months of age, allowing for greater statistical power at this age.

4.4.3 GFAP immunofluorescence in thick 50 µm spinal cord sections

The GFAP immunofluorescence technique offered an alternative way to examine GFAP in thick spinal cord sections. It was carried out on the three genotypes (control, CLN5 and CLN6 affected) utilizing the standard immunofluorescence concentration (1:1,000) which has previously been successful in the Batten disease research laboratory. There are advantages and disadvantages to immunofluorescence over the immunoperoxidase technique. Immunofluorescence is more sensitive but must be performed in the dark, because the fluorescent signal fades over time. On the other hand, the immunoperoxidase method is based on an enzymatic reaction, whilst immunofluorescence is not thus making staining with the latter more consistent between batches. Additionally, immunofluorescence often relies on confocal microscopy to take multiple images down the Z-planes to obtain very detailed images, which may or may not be required. Finally, immunofluorescence might be selected when multiple protein staining is required as this technique allows for colocalisation studies, essential when needing to know what types of cells are expressing what proteins. Here, the immunofluorescent method did not provide a clearer image of glial activation in the affected sheep spinal cord. However, it is possible that the GFAP concentration needed optimisation to truly assess the viability of GFAP immunofluorescence in thick 50 µm spinal cord sections.

4.4.4 Comparison with other NCL models

Reactive astrocytes have been documented prenatally in the CLN6 affected sheep brain, being present in the developing white matter of the cerebral cortex 40 days prior to birth and within the cortical grey matter 20 days before birth [32]. In contrast, the current study indicated that there was no overt astrocytosis in the 3 month CLN5 or CLN6 affected sheep spinal cord, although it appeared to be present in the 18 month samples from CLN6 affected sheep. Analysis of more spinal cord samples across the disease course, as well as using quantitative threshold image analyses, might help to confirm this result.

An unpublished study by Kwan et al has investigated astrocytosis in the CLN6 affected Merino sheep spinal cord [70]. The authors concluded that there was actually less gliosis in the affected white matter compared to healthy control sheep [70]. Gliosis levels were graded from 0 (not present), 1 (mild), 2 (moderate) to 3 (marked) based on assessment of astrocytes in the white matter of thin (3 μ m) haematoxylin and eosin-stained sheep spinal cords. However, this study was only performed at a single timepoint, using spinal cord samples from affected sheep aged between 14 and 17 months of age and comparing them to much older (42-month-old) control sheep, who may have had established age-related astrocytic activation. The authors only looked at the white matter, and not at the grey matter, thus making it difficult to draw comparisons to the current study in CLN5 and CLN6 affected sheep spinal cords. It would seem though that the white matter findings of Kwan et al in CLN6 Merino sheep are in contrast to the findings of this thesis in CLN6 South Hampshire sheep [70].

There are multiple studies investigating astrocytosis in CLN1 affected mice, utilizing the two different immunohistochemical techniques, and all reveal progressive astrocytosis in this murine NCL model identical results[4, 18, 68]. This certainly does not occur to the same extent in the CLN5 or CLN6 affected sheep spinal cord and possible reasons for that will need to be explored further.

4.4.5 Conclusions

- GFAP immunohistochemistry on 50 μ m spinal cord sections failed to detect a significant difference between control and CLN5 and CLN6 affected sheep.
- GFAP immunohistochemistry on 3 μ m spinal cord sections provided a clearer image of cellular morphologies, and revealed an increase in activated astrocytes in the CLN6 affected sheep spinal cord between 3 and 18 months of age, whilst there was a reduction in GFAP immunopositivity in control and CLN5 affected spinal cords over the same time period.
- GFAP immunofluorescence did not provide a clearer picture of astrocytosis in affected spinal cords, although a dilution series may prove useful.
- Batch processing of all samples or the inclusion of a batch control is important in immunohistochemistry to prevent inter-batch variation and allow for accurate analyses.

Chapter 5

Exploring other pathology in the NCL spinal cord

5.1 Introduction

Motor and sensory neurons and astrocytes are not the only cells in the spinal cord. Microglia and interneurons are other important cell populations, and their function can become dysregulated in neurodegenerative conditions like NCL.

Interneurons are important neurons in the spinal cord. As their name suggests, they connect the spinal motor and sensory neurons. Subpopulations of interneurons can be characterised by the calcium binding proteins they express. Parvalbumin (PV), Calbindin D28k (CB) and calretinin (CR) are the three major calcium binding proteins found in morphologically distinct interneurons, and these serve to maintain calcium homeostasis in neurons, and buffer free intracellular calcium [90-92]. The expression pattern of these interneuron subtypes in the spinal cord has been well described in different species [92-100], but there is little in the literature on sheep.

Microglia are highly motile cells in the central nervous system (CNS). They act as immune cells, producing inflammatory cytokines and engaging in the phagocytosis of apoptotic, dead and dying cells. The lectin, I-B4 from *Griffonia simplicifolia* (GSB4) has been successfully used as a microglial marker in brain tissue from NCL affected sheep to visualise activated and inflamed microglia [34]. In CLN5 affected (*CLN5*^{-/-}) and CLN6 affected (*CLN6*^{-/-}) sheep brains, quiescent microglia become activated, increasing in size, with an enlarging cell soma and short thickened processes, typical of brain macrophage-like morphology [35]. This microglial activation is regionally specific and is associated with the progression of neurodegeneration and clinical symptoms [32].

Microglial and interneuron populations have not been well described in either the healthy or NCL diseased sheep spinal cord. In order to do this, a thorough understanding of spinal cord anatomy was required. In addition to the spinal cord being split into grey and white matter, and dorsal and ventral horns, as discussed in Section 1.5.1, these regions can also be sub-divided based on the characteristics and function of their populating cells (Figure 5.1).

The white matter of the spinal cord is primarily composed of bundles of both ascending and descending myelinated axons, and some glial cell bodies [58]. It is divided into the posterior column (or dorsal funiculus), anterior column (or ventral funiculus) and lateral column [101] as seen in Figure

5.1. Axonal fibres within each of these funiculi often have a specific function, for example the fasciculus gracilis and fasciculus cuneatus tracts within the dorsal funiculus mediate position, vibratory and light touch sensation [101].

The grey matter is made up of neuronal cell bodies, glial cells and blood vessels and is split into two dorsal and two ventral horns [58]. The dorsal horns primarily contain interneurons that receive and process somatosensory information that enters the spinal cord via the dorsal roots [59, 60]. The ventral horns are comprised of visceral and somatic motor neuron cell bodies [60], which send axons via the ventral roots to terminate on striated muscles [59]. Small spinal interneurons are found within both of these horns, relaying signals between the sensory and motor neurons.

The grey matter can be further divided into layers or Rexed laminae, which are laid out in the precise order as observed in Figure 5.1. The dorsal horn is comprised of laminae I-V moving anteriorly [58]. Many tightly packed interneurons are found in laminae II-III. Lamina VI contains motor neurons and intersects with the intermediolateral nucleus (Figure 5.1, green), a prominent collection of neurons involved in the sympathetic nervous system, essential for responding to dangerous or stressful situations [58]. Laminae VII and VIII make up the majority of the ventral horn and are the locations where most interneurons are found, Laminae VIII also has motor neurons. Lamina IX exists as a semi-circle section on the anterior side of the ventral horn, and lamina X surrounds the spinal canal through which cerebrospinal fluid flows. Laminae IX consists of both interneurons and motor neurons, which are responsible for spinal reflexes from the descending tracts of the brain [101].

This chapter reports a trial of four different antibodies (PV, CB, CR and GSB4), which are markers for interneuron subtypes and microglial cells. The aims were to first characterise their expression in the normal healthy sheep spinal cord and then compare protein expression in healthy control and CLN6 affected sheep spinal cord at a single timepoint.

Material removed due to copyright compliance

Figure 5.1 Cross-sectional view of the spinal cord

The grey matter is divided into ten distinct Rexed laminae labelled I-X. Within these, there are prominent nuclear groups (indicated in blue, green and red). The white matter is divided into three columns or funiculi, which also contain specific groups of fibres arranged into fasciculi or tracts (as indicated). The image is modified from BioRender, Wikipedia and [58].

5.2 Materials and Methods

Cervical spinal cord samples from a single 18-month-old healthy control and a 15-month-old CLN6 affected sheep were used in this experiment. All immunohistochemical staining, except for GSB4, utilized the same procedure as described in Section 2.6.2 and the corresponding primary and second antibodies are shown in Table 5.1. The GSB4 protocol was as follows. 50 µm spinal cord sections underwent blocking for 30 mins and 1 h respectively in 1% in 50% methanol in PBS and then 15% normal goat serum in PBST. Sections were incubated in biotinylated GSB4 lectin (1:500, B-1205, Vector Laboratories, Newark, CA, USA) in 10% normal goat serum in PBS-T, 24 h, 4°C. Colour detection was performed by incubation in ExtrAvidin Peroxidase (1:1000, Sigma, E-2886) diluted in PBS-T, 4 h, prior to the application of diaminobenzidine tetrahydrochloride (DAB, D5637, Sigma-Aldrich), 5 mins. Sections were mounted in chrome alum solution, air-dried, and then cover-slipped with DPX. Images were collected on the Nikon Eclipse 50i microscope, using the 10X objective in both

the dorsal and ventral horn, to visually assess the immunoreactivity of each antibody in the sheep spinal cord.

Table 5.1 Primary and secondary antibodies used in this study

Antibody name	Primary Antibody	Secondary Antibody, 1:1000 dilution	DAB incubation time (min)
Parvalbumin (PV)	1:5000, Swant235, Swant, Bellinzona, Switzerland	Goat anti-mouse IgG, B7151, Sigma	7
Calbindin (CB)	1:5000, Swant 7699/4	Goat anti-rabbit IgG, B7389, Sigma	5
Calretinin (CR)	1:2000, Swant 300	Goat anti-rabbit IgG, B7389, Sigma	7

5.3 Results

Characterisation of antibody staining in the sheep spinal cord was first performed by visual observation of the control sections before comparison with CLN6 affected sections. A gross description was made, then white matter and grey matter regions were assessed. Details outlining the neurochemical distribution is provided (Table 5.2, Figure 5.5,) and then each immunostain is discussed separately.

Table 5.2 Qualitative assessment of calcium binding protein immunoreactivity in the 18 month old healthy sheep cervical spinal cord

Cell population	Dorsal horn grey matter	Ventral horn grey matter	Dorsal white matter	Ventral white matter
PV	Puncta in IV-VI	Intense neuropil in X, puncta in VII-VIII, sparse large PV-positive cells in VIII	Intense neuropil in fasciculus gracilis	Intense neuropil on grey matter boundary
CB	Intense neuropil staining and CB-positive cells in I-III	Moderately stained CB-positive cells in VII-IX	Lattice pattern with axonal puncta and some small CB-positive neurons laterally	
CR	Mild neuropil staining and small CR-positive cells in I-II	Lightly stained CR-positive cells in VII-IX	No obvious CR-positive cells	

5.3.1 Parvalbumin expression in the sheep spinal cord

Macroscopically, the parvalbumin (PV) stained healthy control sections displayed an obvious triangular cluster of intense neuropil and fusiform staining in the dorsomedial aspect of the white

matter, in the region known as the fasciculus gracilis, as well as similar pockets in the grey matter lamina X, ventral to the central canal.

Microscopically, these triangular clusters in the dorsal funiculus were found to contain intense neuropil staining alongside PV-positive cells with a fusiform morphology and some punctate circular axonal staining. This staining cleared laterally to just circular axonal puncta with no obvious cellular or neuropil staining. In the ventral white matter, the same fusiform morphologies were observed, with more intense neuropil staining close to the grey matter – white matter boundary (Figure 5.2).

Assessment of the dorsal horn grey matter revealed that the first three superficial Rexed laminae (I-III) were devoid of staining, while diffuse neuropil staining was observed in the deeper dorsal laminae (IV-VI), with some small intensely stained PV-positive puncta but no obvious cell bodies (Figure 5.2A). In the ventral horn, there was neuropil staining across all laminae (VII-IX) and some sparse lightly stained larger cell bodies (Figure 5.2B). These were neuronal in morphology and typically bipolar or multipolar. Higher magnification confirmed the presence of tiny spherical PV-positive puncta in the same laminae but there was no easy way to quantify them. The greatest level of PV-positive immunostaining in the ventral horn was seen in lamina X and consisted of intense neuropil staining and the same fusiform cellular morphology seen in the ventral white matter.

There were few qualitative differences when comparing parvalbumin staining in the control and CLN6 affected sheep spinal cords (Figure 5.5), except that the affected dorsal horn did not have the band devoid of staining in laminae I-III, but rather very diffuse neuropil staining with little to no puncta in the entire horn.

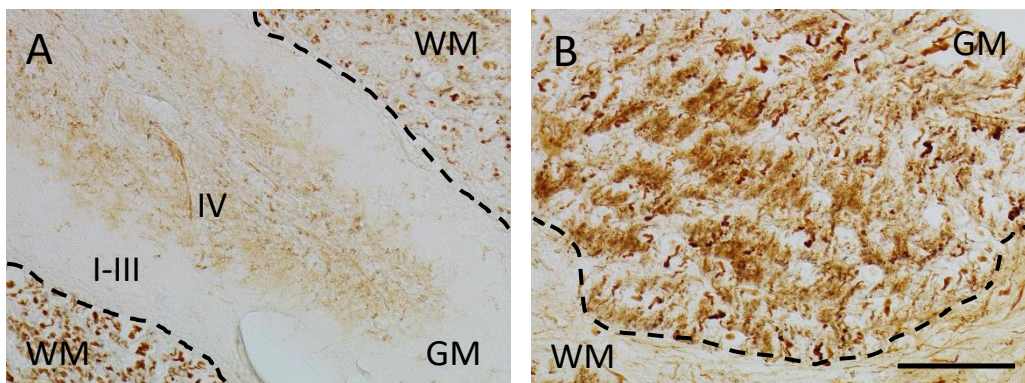


Figure 5.2 Parvalbumin immunoreactivity in the healthy sheep spinal cord

A. Intense neuropil staining in the fasciculus gracilis dorsal white matter (bottom left), no staining in laminae I-III and some PV-positive puncta in deeper laminae of the dorsal horn grey matter. B. Intense neuropil staining and puncta in the grey matter of the ventral horn. The dashed lines delineate the grey matter/white matter boundary. Scale bar represents 50 μm .

5.3.2 Calbindin expression in the sheep spinal cord

Macroscopic inspection of the calbindin (CB) stained healthy sheep spinal cord revealed that the dorsal horn was more darkly stained than the ventral horn, and a lattice pattern was observed in the white matter, which was comprised of myelinated nerve fibres (axons).

Microscopic assessment showed an obvious gradient of staining in the dorsal horn grey matter, with intensely stained neuropil and CB-positive cells in laminae I-III (Figure 5.3A). The stained cells appeared to be neuronal in morphology but they were hard to visualise against the background neuropil so an adjustment to the CB antibody concentration might allow for confirmation.

Comparatively, the ventral horn grey matter had a more even distribution of moderate neuropil staining, with some light to moderately stained CB-positive cells which also had typical neuronal morphology (Figure 5.3). It is plausible that these were large interneurons, although double labelling immunofluorescence with CB and NeuN may aid in distinguishing them from motor neurons.

Within the lateral columns of the white matter (lateral and anterolateral funiculi), there was an intensely stained lattice and some clear but small CB-positive neurons. In the white matter adjacent to the dorsal and ventral horns, there was a lattice pattern reminiscent of the cross-sectional appearance of axonal fibre bundles (Figure 5.3C). This morphed dorsally and laterally to more diffuse neuropil staining with some immunopositive fusiform-like structures also present.

Macroscopically, the affected spinal cord appeared similar to the control. The neurochemical expression pattern was uniform throughout the white matter in both the healthy and affected spinal cord (Figure 5.5). Microscopically, all regions were comparable to the healthy control cord, except that there appeared to be fewer fusiform structures in the fasciculus gracilis and anterior funiculus of the white matter and fewer CB-positive cells in the ventral horn. Quantification of cell number would be required to confirm this observation.

Material removed due to copyright compliance

Figure 5.3 Calbindin expression in the healthy sheep spinal cord

A. Neuropil staining in the dorsal horn was intense, making it difficult to see CB-positive cells. Dashed lines represent the start of lamina I (bottom) and end of lamina III (top). B. Large CB-positive cells with neuronal morphology were present in the ventral horn (arrows). C. The white matter lattice pattern, with cross-sectional axonal morphology. Scalebar represents 50 μm (A,B) and 100 μm (C).

5.3.3 Calretinin expression in the sheep spinal cord

Macroscopic examination of the calretinin (CR) stained sections revealed very light staining compared to the other interneuronal markers, suggesting that the antibody concentration may require optimisation. However, there was a distinctly darker staining pattern in the grey matter compared to the white matter with no obvious staining in the mediodorsal white matter (fasciculus gracilis).

Microscopic examination of the grey matter in the healthy sheep dorsal horn revealed superficial laminae I-II neuropil staining with scattered small CR-positive multipolar cells, some of which had immunopositive processes (Figure 5.4A). Only extremely light neuropil staining was detected in the deeper dorsal horn laminae (III-V). The grey matter in the ventral horn possessed diffuse neuropil and sparse punctate staining, with some larger CR-positive cells which were only lightly stained (Figure 5.4B). There was no staining in the dorsal white matter, while ventral white matter presented with a light lattice staining pattern of the cross-sectional profile of axons, similar to the calbindin staining.

Comparison of the CR stained spinal cord between healthy and CLN6 affected sheep indicated that the affected spinal cord appeared to be less stained than the healthy control spinal cord (Figure 5.5). Staining in the dorsal horn grey matter was less intense in the affected spinal cord, but the same CR-positive cells were observed in the superficial laminae I-II. There appeared to be fewer CR-positive cells in the affected ventral horn. There was no obvious lattice pattern in the affected white matter, which was seen in the healthy control, but rather diffuse neuropil staining and the presence of fusiform spindles.

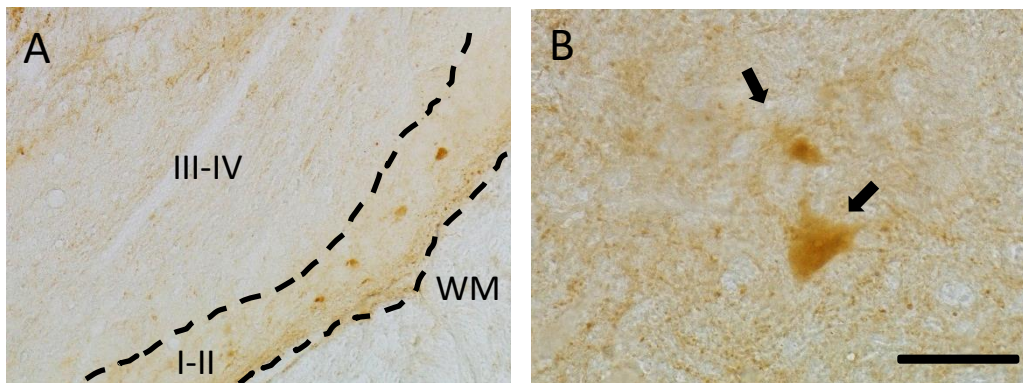


Figure 5.4 Calretinin expression in the healthy sheep spinal cord

A. CR-positive cells were present in a lamina-specific distribution, in laminae I-II of the dorsal horn. B. Large CR-positive cells were also detected in the ventral horn (arrows). Scalebars represent 100 μm (A) and 50 μm (B).

5.3.4 GSB4 expression in the sheep spinal cord

On macroscopic examination of the GSB4 stained healthy sheep spinal cord sections, a stereotypical white matter lattice pattern was evident as well as diffuse neuropil staining in the grey matter as evident in Figure 5.5 below. The white matter staining showed a lattice-like pattern similar to what was observed with CB and CR (Figure 5.5).

There is only diffuse neuropil staining in the ventral horn, which was also present in the dorsal horn, although the latter had a gradient of expression with the highest neuropil staining on the medial surface.

When the healthy control and CLN6 affected GSB4-stained sections were compared, there were no differences observed except for the staining intensity. Surprisingly, there was no specific cellular staining in the grey matter in either sample, although GSB4-positive activated microglia and/or macrophages can be seen in the affected sheep brain. Equally there was no staining in the white matter, which is where macrophages and glial cells typically reside.

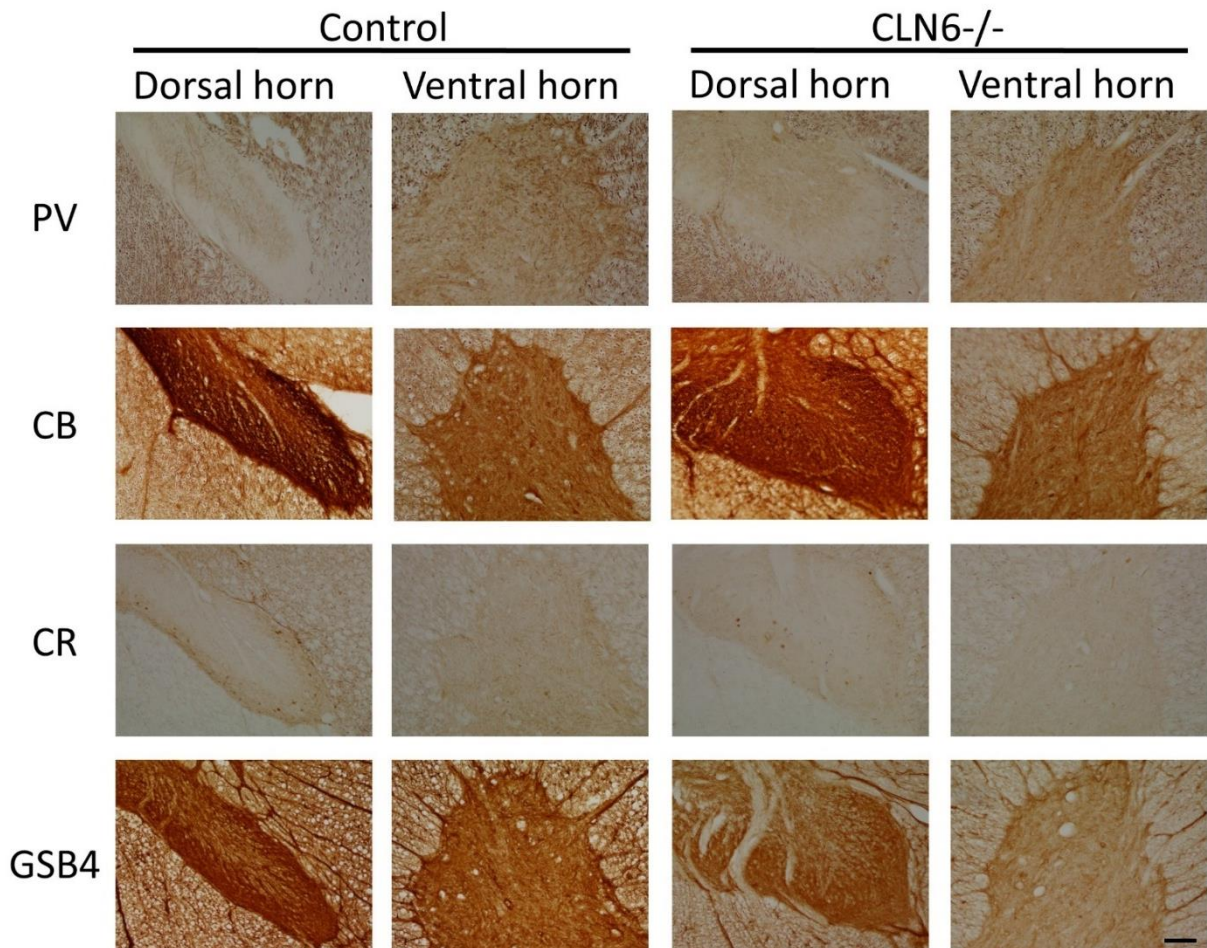


Figure 5.5 Summary of the control and affected immunohistochemistry staining
 Representative images of interneuron and microglial staining in the sheep spinal cord. 18-month-old healthy control and 15-month-old CLN6 affected (*CLN6^{-/-}*) cervical spinal cord sections were stained with parvalbumin (PV), calbindin (CB), calretinin (CR), and biotinylated α -D-galactose specific isoelectin 1-B4 (GSB4) and the expression pattern compared. The scale bar represents 100 μ m.

5.4 Discussion

Interneurons and microglia are important cells within the CNS, yet their expression pattern varies across animal species and has not been well described in sheep. Here, a preliminary immunohistochemical investigation was performed using a microglial marker (GSB4) and key interneuron markers (PV, CB and CR) to investigate their neurochemical distribution in healthy and CLN6 affected sheep spinal cord. This discussion will summarise the findings on the patterns of PV-positive, CB-positive and CR-positive expression in the sheep spinal cord and each of these will be discussed separately and compared to other animal species and/or humans. The expression profile of GSB4 in the sheep spinal cord will also be discussed, with a particular focus on comparisons between healthy and CLN6 affected sheep, and with other animal models of NCL.

5.4.1 Parvalbumin distribution in sheep spinal cord and other species

In the sheep spinal cord, PV-positive staining was concentrated in the neuropil of the dorsomedial white matter, tiny spherical puncta in the deeper dorsal and ventral grey matter laminae (IV-VI and VII-VIII) and sparse large cells in lamina VIII of the ventral horn.

PV-positive expression in the spinal cord of other species is quite varied. It appears both superficially in the dorsal horn and then in the deeper laminae (VII-VIII) in the ventral horn of rats, particularly in a region known as the dorsal nucleus in lamina VI [98]. However, there are distinct pockets of intense PV-positive cells in laminae III and IV in dogs [102] and in laminae IV-VIII in cats [103]. Like sheep, mice also have large PV-positive cells in the ventral horn [99], whilst the fusiform morphologies seen in the sheep white matter resemble those seen in the same region in rats [98].

5.4.2 Calbindin distribution in sheep spinal cord and other species

The most distinct calbindin-expressing interneurons in the sheep spinal cord existed in a clear band in grey matter laminae I-III of the dorsal horn. Some less intensely stained CB-positive cells, with clear neuronal morphology, were present in the ventral horn grey matter as well as the lateral white matter.

Like sheep, there is an intensive zonal distribution of CB-positive cells, which has been documented in the superficial laminae I-III of the dorsal horn in mice, rats, cats and dogs [93, 98, 99, 102, 103]. Whilst expression is very sparse in the ventral horn of mice [99], rats have higher expression in the deeper laminae of the ventral horn [98]. The CB-positive cells in sheep appear to be neuronal in morphology, but some future optimisation of the antibody concentration or double-labelling with a neuronal marker like NeuN might confirm this. Currently little has been reported for CB-positive expression in the white matter of the spinal cord in other animal species.

5.4.3 Calretinin distribution in sheep spinal cord and other species

Like CB-positive, CR-positive expression in the sheep spinal cord is predominantly in the superficial laminae I-III of the dorsal horn. Some larger, but less immunopositive, cells were also detected in the ventral grey matter.

One paper compared CR-positive expression in mice, rats, and humans [104], all of which presented a similar staining pattern to that observed in sheep. In all four species, there is a zone of highest expression in laminae I-III [99, 104], whilst there is a lack of expression around the central canal in

mice [104]. However, in rats, cats and dogs most CR-positive expression is in the deeper layers of the ventral horns [98, 102, 103].

5.4.4 GSB4 distribution in sheep spinal cord

Previous reports have suggested that the GSB4 lectin is not effective at detecting microglial populations in the sheep spinal cord (Professor Jon Cooper, personal communication). No specific cellular staining of GSB4-positive microglia or macrophages was detected in the spinal cord in the current study. It might still be useful in the future to attempt a dilution series to categorically confirm that this lectin is ineffective in the sheep spinal cord.

5.4.5 Comparison of interneuron and microglial expression patterns between control and affected sheep spinal cord.

Surprisingly, there was no apparent differences in expression patterns for any of the interneuron or microglial markers between the healthy and CLN6 affected sheep. In this study the samples utilized were a 15-month-old CLN6 affected and 18-month-old healthy control sheep. Therefore, one possible reason why there is minimal difference between the control and affected CLN6 samples could be their different ages. Based on the results presented in Chapter 3, pathology in the ovine NCL spinal cord occurs quite late in the disease process (~18 months of age) and there was no discernible difference between healthy control and CLN6 affected motor neuron counts at 12 and 18 months. In future, it will be useful to test these antibodies on more animals and at later ages (≥ 18 months) to see if a difference in interneuron numbers emerges.

Additional optimisation of the antibodies is required to enhance the staining and potentially increase what can be visualised in the sections. In particular, GSB4 and calbindin sections were overstained, so a dilution series should be attempted to reduce background staining, whilst the calretinin staining was very faint hence its concentration should be increased. Additionally, the immunohistochemical staining revealed large PV-positive, CB-positive and CR-positive cells within the ventral horn with typical neuronal morphology, and double labelling with NeuN would be useful to distinguish them from motor neurons.

The expression of all three interneuron subtypes has been explored in the CLN6 diseased sheep brain [34]. PV-positive cells are lost in the affected sheep cortex as early as 4 months of age, whilst CB-positive neuronal populations remain well preserved, and CR-positive neurons actually increase until end-stage disease (19 months of age). Similarly, interneuron populations have been explored in the

brain and spinal cord of CLN1 affected mice. Examination revealed extensive interneuron loss in the cortex, while hippocampal interneuron populations were also vulnerable to loss [69, 79-81]. Further studies on the CLN1 affected spinal cord revealed a significant overall reduction in PV-positive, CB-positive and CR-positive cell counts [4]. Thus demonstrate an early and selective loss of spinal interneurons in the CLN1 affected mice from 2 months of age [4].

The lectin GSB4 has successfully been used in the brain as a microglial marker, to show a prominent activation response as early as 12 days old in CLN6 affected sheep [34]. There is very little difference in the structure of the grey matter in the brain and spinal cord, so the lack of GSB4 reactivity in the sheep spinal cord was an unanticipated result. A further immunohistochemical dilution series would confirm its ineffectiveness. An alternative microglial marker (CD68) has been used in CLN1 affected mice to show an expression of CD68-positive stain with both the dorsal and ventral horn of affected mice as early as 1 month and therefore signifies that astrocytes and microglia are activated very early in the disease progression [68]. Since CD68 is effective in the spinal cord of the mice, CD68 staining could also be attempted as a method for visualising microglia in the sheep spinal cord.

5.5 Conclusions

- Parvalbumin immunohistochemistry revealed intense neuropil staining in the dorsomedial white matter, tiny spherical puncta in laminae IV-VI and VII-VIII and sparse large cells in lamina VIII of the sheep spinal cord. The distribution of PV-positive interneurons is varied across species, although there is some overlap between sheep, cats, dogs and mice.
- Calbindin immunohistochemistry revealed a clear band of CB-positive cells in the grey matter laminae I-III, which is the same as that observed in mice, rats, cats and dogs. Some CB-positive cells in the ventral horn and lateral white matter also had neuronal morphology.
- Calretinin expression is predominantly in the superficial laminae I-III of the dorsal horn and deeper laminae VIII and IX of the ventral horn, which is a similar pattern to that observed in mice, rats, and humans.
- There was little to no difference in expression pattern between healthy 18-month control and 15-month-old CLN6 spinal cord samples. It would be useful to optimise the PV, CB and CR antibodies and try them on samples from more, and older, animals.
- GSB4 does not appear to detect microglial populations in the sheep spinal cord, although a future dilution series will definitively determine its effectiveness. Alternative microglial markers, like CD68, might prove better.

Chapter 6

Discussion and Conclusions

Neuronal ceroid lipofuscinosis (NCL) is a fatal, recessively inheritable, neurodegenerative lysosomal storage disorder that affects approximately 1 in 12,500 children worldwide [1]. Currently there are 13 known variants of NCL, caused by mutations in the genes *CLN1-8* or *CLN10-14*, which all express the same clinical symptoms including progressive mental and motor deterioration, blindness, epileptic seizures, and premature death [15]. There are many established animal models of NCL, including naturally occurring CLN5 and CLN6 forms in Borderdale and South Hampshire sheep breeds respectively [24, 28]. These two models have been instrumental in a better understanding the human condition and the development of gene therapies. Affected sheep already have well-characterised brain and retinal pathology which consists of progressive neurodegeneration, neuroinflammation, storage accumulation, and blindness [24, 34, 35, 105], however, very little is known about their corresponding spinal cord pathology and what impact this might have for treatment. Therefore, this study set out to examine spinal cord pathology in CLN5 and CLN6 NCL sheep models.

6.1 Spinal cord anatomy and neurochemistry in the healthy sheep spinal cord

It was first important to characterise any anatomical, neurochemical or pathological changes in the healthy sheep spinal cord over time, to then be able to compare these to the CLN5 and CLN6 affected spinal cords. Thus, this study presents a histopathological review of the normal sheep spinal cord, which to the best of our knowledge, has not been documented before.

Visual examination of the healthy sheep spinal cord showed that it was cylindrical to oval in shape over its full length. It was at its greatest width and depth in the cervical region, reducing in both parameters through the thoracic region, before increasing in total area again through the lumbar spine. Area measurements in the healthy sheep spinal cord over time revealed a near linear increase in total cross-sectional area and white matter area across all three spinal cord regions (cervical, thoracic and lumbar). These did not begin to plateau over the current study, even at the oldest timepoint studied, indicating that the sheep and therefore their spinal cords had not reached maturity or finished growing by 18 months of age. Importantly, there was little change in healthy spinal grey matter volume between 3 and 18 months of age, which fits with the theory that “we are born with all the neurons we will ever have”. Motor neuron counts in the ventral horn consolidated

this idea, as there was little increase in their numbers in healthy sheep between ages 6, 12 or 18 months of age. Whilst there have been some reports of spinal cord neurogenesis (production of new spinal neurons) following injury [106, 107], this phenomenon is believed to only occur at a low rate under normal conditions [108]. Therefore, the total and white matter area increases seen here in the healthy sheep spinal cord could more likely be attributed to axonal maturation and development of mature myelination.

Glial and interneuron populations have not been well described in the healthy sheep spinal cord. Immunostaining with an astrocytic marker, GFAP, showed that there was no significant change in the astroglial population over time. Healthy astrocyte levels remained constant over time and were present in the sheep spinal cord as two clear morphologies, being protoplasmic with large cell bodies and many branching processes in the grey matter, and fibrous with smaller cell somata and processes that aligned with the myelinated fibres of the white matter lattice. A microglial marker, GSB4, did not appear to detect healthy quiescent microglial populations in the sheep spinal cord, however immunohistochemistry with interneuron markers (parvalbumin, calbindin and calretinin) provided a clear picture of their distribution. Parvalbumin-positive interneurons were mainly located in deeper Rexed laminae IV-VIII of the spinal grey matter, whilst calbindin- and calretinin-positive interneurons were present in clear bands in the more superficial laminae I-III of the dorsal horn.

Finally, as NCL is a lysosomal storage disease, it was necessary to confirm if intracellular fluorescent material or “aging pigments” like lipofuscin [109] accumulated in the aging sheep spinal cord. This study concluded that there were no fluorescent aggregates in the healthy sheep spinal cord, even at 18 months of age, thus making it an excellent control for NCL affected samples.

6.2 Spinal cord pathology in the NCL affected sheep spinal cord

The current study is the first to document neurodegeneration, neuroinflammation and lysosomal storage body accumulation in the spinal cord of CLN5 and CLN6 affected sheep. It provides a timeline of these spinal cord pathologies in the sheep (Figure 6.1), which will be compared to clinical symptoms and documented brain pathology in Section 6.3.

Measurements of the total cross-sectional, grey and white matter areas gave an indication of atrophy in the affected sheep spinal cord. Whilst there was no loss in grey matter area for either genotype over time, total area and white matter area measurements increased over the disease course, until 18 months of age when there was a dramatic reduction. Motor neuron counts remained constant in

the CLN6 affected sheep spine, yet there was a late-stage reduction in the caudal spine (thoracic and lumbar regions) between 12 and 18 months of age in CLN5 affected sheep. Interneuron populations were examined at a single timepoint (15 months of age) and there was no obvious difference between control and affected samples. These findings indicated that the affected sheep spinal grey matter was well preserved and suggested that any changes in neuron numbers occurred late in the disease course. White matter changes also appeared to be a late-stage phenomenon and could be indicative of loss of axons and myelin sheaths but this would need to be explored further.

The accumulation of intracellular fluorescent storage bodies is a key pathological finding in NCL. Lysosomal storage is reported to be ubiquitous across the body, and this study showed that it accumulated linearly and to a greater degree in the CLN6 affected spinal cord, whilst the increases were much more modest in CLN5 affected sheep, until 18 months of age (again late-stage disease) when there was a dramatic increase in fluorescence in the spinal grey matter.

Neuroinflammation has been reported to be a precursor for neurodegeneration in the brain of CLN5 and CLN6 affected sheep [34, 35], hence immunohistochemistry with the astrocytic marker, GFAP, was tested on sheep spinal cord sections. There was no significant difference in GFAP immunostaining between control, CLN5 and CLN6 affected sheep in the thicker 50 μ m sections but it was difficult to see individual cells against the intensely stained neuropil. The thin 3 μ m sections provided a clearer indication of cellular morphologies and showed an increase in activated astrocytes in the CLN6 affected spinal cord between 3 and 18 months of age, which was not apparent in the CLN5 affected samples over the same period.

Collectively these results show that manifest spinal cord pathology in NCL affected sheep typically occurs in the later stages of the disease (15 to 18 months of age). While some neuron loss and lysosomal storage did occur earlier (from 6 - 12 months of age), these did not become overt until 18 months of age. Some spinal cord pathology occurred earlier and to a greater extent in CLN6 affected individuals, including lysosomal storage accumulation and neuroinflammation, yet total cross-sectional area, white matter area and motor neuron counts were more impacted by CLN5 disease. However, it was interesting to note that spinal pathology in the two ovine disease models were very similar at 18 months of age for all parameters assessed, except motor neuron count. This suggests that despite some subtle differences in the pathogenic cascade in the spinal cord, the pathological endpoint for the two disease models was the same.

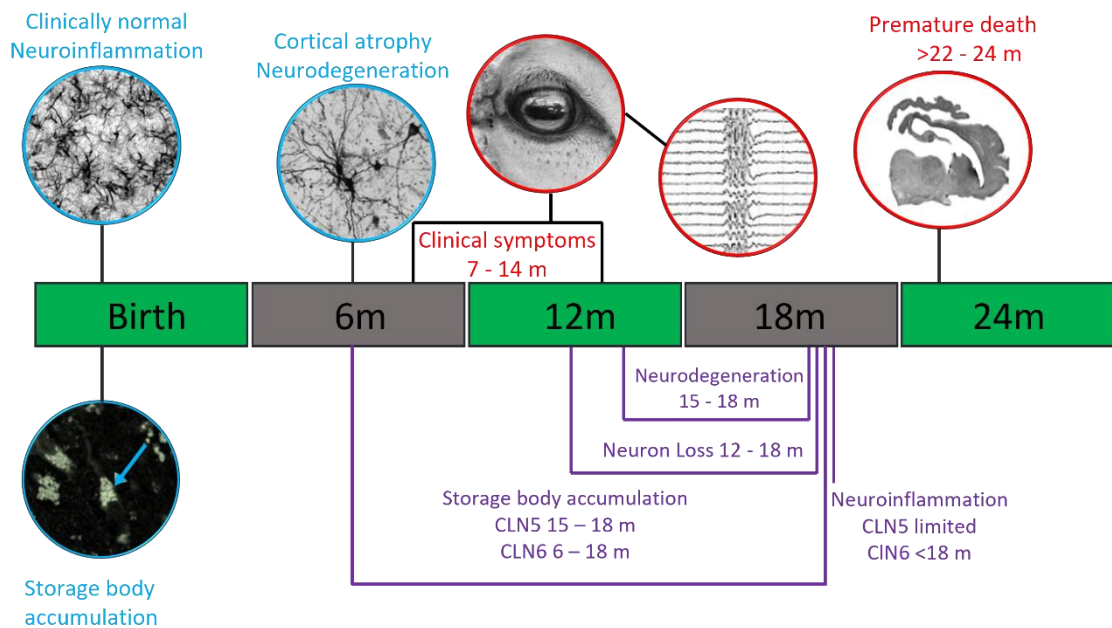


Figure 6.1 A timeline of clinicopathological changes in the CLN5 and CLN6 ovine NCL models. Pathological changes in the brain (blue text) precede clinical symptomatology (red text). Spinal cord pathology determined in the current study is documented in purple and appears to occur later in the disease process.

6.3 Comparison of spinal cord pathology, brain pathology and clinical symptoms in ovine NCL

Figure 6.1 provides a schematic of the timeline of key clinicopathological features of ovine NCL. The earliest documented pathology is glial activation which occurs prior to birth in the cortical grey and white matter of the brain [32]. This begins in regions most susceptible to later neurodegeneration but does extend with time to cover most of the cortical mantle [34, 35]. Lysosomal storage is present as early as 12 days old in the affected sheep brain and becomes more widespread with age [34]. Neurodegeneration has not been documented to occur until around 6 months of age, and is regionally selective, beginning first in the primary visual and parieto-occipital cortices [34, 35]. However, it should be noted that all of these key pathological characteristics present before the onset of clinical symptoms (7-14 months of age) in CLN5 and CLN6 affected sheep [35, 36]. Affected sheep lose vision from 9 months of age, cognitive, proprioceptive and motor deficits begin from 12 months of age and become progressively worse as the sheep age, and premature death occurs before 24 months of age [35]. The findings from this thesis have been included into this timeline (Figure 6.1) to show that spinal cord pathology appears to be a secondary pathology which occurs significantly after the brain pathology. Although lysosomal storage in the CLN6 affected sheep spinal cord increased linearly from 3 months of age, it did not increase dramatically until 18 months of age in the CLN5 affected spine, at a similar timepoint to spinal neurodegenerative changes.

Neuroinflammation in the spinal cord was also increased at 18 months of age but, as it was only assessed at two timepoints, analysis of further spinal cord samples over the disease course will be required to pinpoint at which age this begins.

Loss of motor and sensory neurons, or white matter tracts, in the spine can result in muscle weakness (paresis), loss of motor control, loss of sensory signalling to the brain, and at worst generalised paralysis [88, 106]. Affected sheep do not exhibit severe motor dysfunctions, like akinesia and dyskinesia, until late in the disease (18 months of age or older [35]) and not all sheep experience these symptoms. Thus, it stands to reason that spinal cord pathologies which might impact on motor activity and sensation would be a late-stage phenomenon as observed in this study. Indeed, atrophic changes in the primary motor cortex of CLN5 and CLN6 affected sheep do not occur until this stage too, much later than neuronal loss in regions associated with early symptomology, such as the primary visual cortex [35].

6.4 Comparison with other NCL models

It has been well documented that spinal cord pathology in CLN1 mice precedes the brain pathology [4, 18, 68]. This led these researchers to describe a “bottom-up” or “body-first” propagation of disease in this NCL mouse model, with disease starting in the body and progressing to the brain [110]. In particular, the first disease manifestations start in the sensory nerves and spinal interneurons, then make their way into the brainstem and around different regions of the brain before impacting the optic nerve and retina [110]. However, in contrast, the CLN5 and CLN6 ovine models used in the current study appear to have a “top-down” or “brain-first” spread of pathology, which matches the propagation pattern postulated for CLN3 disease [110]. Pathology presents first in the retina of CLN3 affected mice, then progresses into the occipital connectome of the CLN3 affected brain before theoretically reaching the peripheral motor neurons of the spinal cord [110]. For CLN5 and CLN6 affected sheep, it is postulated that the first pathologies begin in the brain [34, 35] and then make their way to the periphery, impacting the retina [105] and the spinal cord (current study) later in the disease course.

6.5 Implications for therapy

As detailed in Section 1.4.1, the CLN5 and CLN6 sheep models have been used to develop and validate gene therapies, with the hopes of expanding the length and quality of life for human patients affected by these NCL forms. Adeno-associated viral vectors (AAV) carrying a functional copy of the mutant NCL gene have been delivered intracerebroventricularly (into the lateral ventricles of the brain) and transduced cells throughout the affected sheep brain and along the full extent of the

spinal cord [37, 50, 52] (Nadia Mitchell, personal communication). In particular, intracerebroventricular delivery of CLN5 gene therapy has slowed or halted disease progression, extended lifespan and corrected disease pathology [37, 50, 52].

Similar studies have been performed in CLN1 mice [4]. Intracranial delivery of AAV vectors carrying a functional copy of the *CLN1* gene resulted in histopathological correction in the brain, but no impact on the spinal cord pathology. Intrathecal delivery into the CSF in the lumbar spine had the reverse effect, correcting the spinal cord. Targeting both the brain and spinal cord with dual intracranial and intrathecal administration resulted in synergistic improvements in lifespan and motor function.

It seems likely that in NCL models, like CLN1, which follow the “bottom-up” propagation of disease that both the brain and spinal cord will need to be treated, either systemically or by a combined intrathecal and brain-directed therapy strategy. In CLN3, CLN5 and CLN6 forms, with their potential “top-down” propagation, administration of a gene therapy into the CSF in the brain may be sufficient to correct pathology in both the brain and spinal cord.

6.6 Future directions

This study provides an excellent natural history of spinal cord pathology in the CLN5 and CLN6 ovine models of NCL. It provides data across the disease course (3 to 18 months of age) from healthy and affected sheep which can be used to compare pathology in the spinal cords of sheep who have received brain-directed gene therapies. This will test if the administration of a gene therapy into the CSF in the brain is sufficient to halt or correct pathology in the spinal cord, as well as the brain. Spinal cords have been collected from almost 50 animals that have received AAV-mediated CLN5 and/or CLN6 gene therapy and they will be assessed using the methods developed in this thesis.

The current study developed methods for quantifying total cross-sectional, grey and white matter areas, motor neuron counts and performing threshold image analysis of neuroinflammation and lysosomal storage. These could be extended to quantitatively measure all spinal cord neurons or NeuN-positive areas per horn. Some fine-tuning of the immunohistochemical procedures for GFAP-positive astrocytes (Chapter 4), GSB4 or CD68-positive microglia (Chapter 6) and parvalbumin, calbindin or calretinin-positive interneurons (Chapter 6) would provide more data and expand on the knowledge generated by this natural history of spinal cord pathology in CLN5 and CLN6 affected sheep.

References

1. Rider, J.A. and D.L. Rider, *Batten disease: past, present, and future*. American Journal of Medical Genetics, 1988. **31**(S5): p. 21-26.
2. Mole, S., R. Williams, and H. Goebel, *The Neuronal Ceroid Lipofuscinoses (Batten Disease)*. 2011: Oxford University Press.
3. Kohlschütter, A., et al., *Current and Emerging Treatment Strategies for Neuronal Ceroid Lipofuscinoses*. CNS Drugs, 2019. **33**(4): p. 315-325.
4. Shyng, C., et al., *Synergistic effects of treating the spinal cord and brain in CLN1 disease*. Proceedings of the National Academy of Sciences of the United States of America, 2017. **114**(29): p. E5920-e5929.
5. Kousi, M., A. Lehesjoki, and S.E. Mole, *Update of the mutation spectrum and clinical correlations of over 360 mutations in eight genes that underlie the neuronal ceroid lipofuscinoses*. Human Mutation, 2012. **33**: p. 42-63.
6. *UCL - NCL Disease - NCL Resource - A gateway for Batten disease*. 2022: University College London, Gower Street, London.
7. Santavuori, P., et al., *Early juvenile neuronal ceroid-lipofuscinosis or variant Jansky-Bielschowsky disease: diagnostic criteria and nomenclature*. Journal of Inherited Metabolic Disease, 1993. **16**(2): p. 230-2.
8. Santavuori, P., et al., *A variant of Jansky-Bielschowsky disease*. Neuropediatrics, 1982. **13**(3): p. 135-41.
9. Holmberg, V., et al., *Phenotype-genotype correlation in eight patients with Finnish variant late infantile NCL (CLN5)*. Neurology, 2000. **55**(4): p. 579-81.
10. Santavuori, P., et al., *The spectrum of Jansky-Bielschowsky disease*. Neuropediatrics, 1991. **22**(2): p. 92-6.
11. Moore, S.J., et al., *The clinical and genetic epidemiology of neuronal ceroid lipofuscinosis in Newfoundland*. Clinical Genetics, 2008. **74**(3): p. 213-22.
12. Xin, W., et al., *CLN5 mutations are frequent in juvenile and late-onset non-Finnish patients with NCL*. Neurology, 2010. **74**(7): p. 565-71.
13. Sleat, D.E., et al., *Mass spectrometry-based protein profiling to determine the cause of lysosomal storage diseases of unknown etiology*. Molecular & Cellular Proteomics, 2009. **8**(7): p. 1708-18.
14. Sharp, J.D., et al., *Loci for Classical and a Variant Late Infantile Neuronal Ceroid Lipofuscinosis Map to Chromosomes 11p15 and 15q21-23*. Human Molecular Genetics, 1997. **6**(4): p. 591-595.
15. Mole, S.E., R.E. Williams, and H.H. Goebel, *Correlations between genotype, ultrastructural morphology and clinical phenotype in the neuronal ceroid lipofuscinoses*. Neurogenetics, 2005. **6**(3): p. 107-126.
16. Arsov, T., et al., *Kufs disease, the major adult form of neuronal ceroid lipofuscinosis, caused by mutations in CLN6*. American Journal of Human Genetics, 2011. **88**(5): p. 566-73.
17. Davidson, M.K., J.R. Lindsey, and J.K. Davis, *Requirements and selection of an animal model*. Israel Medical Association Journal, 1987. **23**(6): p. 551-555.
18. Nelvagal, H.R., et al., *Pathomechanisms in the neuronal ceroid lipofuscinoses*. Biochimica et Biophysica Acta (BBA) - Molecular Basis of Disease, 2020. **1866**(9): p. 165570.
19. Cooper, J.D., M.A. Tarczyluk, and H.R. Nelvagal, *Towards a new understanding of NCL pathogenesis*. Biochimica et Biophysica Acta (BBA) - Molecular Basis of Disease, 2015. **1852**(10, Part B): p. 2256-2261.
20. Bond, M., et al., *Use of model organisms for the study of neuronal ceroid lipofuscinosis*. Biochimica et Biophysica Acta (BBA) - Molecular Basis of Disease, 2013. **1832**(11): p. 1842-1865.
21. Rosenberg, J.B., et al., *Advances in the treatment of neuronal ceroid lipofuscinosis*. Expert Opinion on Orphan Drugs, 2019. **7**(11): p. 473-500.

22. Faller, K.M., et al., *The neuronal ceroid lipofuscinoses: Opportunities from model systems*. Biochimica et Biophysica Acta (BBA) - Molecular Basis of Disease, 2015. **1852**(10 Pt B): p. 2267-78.
23. Hagen, L.O., *Lipid dystrophic changes in the central nervous system in dogs*. Acta Pathologica et Microbiologica Scandinavica, 1953. **33**(1): p. 22-35.
24. Jolly, R.D., et al., *Neuronal ceroid-lipofuscinosis in Borderdale sheep*. The New Zealand Veterinary Journal, 2002. **50**(5): p. 199-202.
25. Frugier, T., et al., *A new large animal model of CLN5 neuronal ceroid lipofuscinosis in Borderdale sheep is caused by a nucleotide substitution at a consensus splice site (c.571+1G>A) leading to excision of exon 3*. Neurobiology of Disease, 2008. **29**(2): p. 306-15.
26. Jolly, R.D., R.D. Martinus, and D.N. Palmer, *Sheep and other animals with ceroid-lipofuscinoses: their relevance to Batten disease*. American Journal of Medical Genetics, 1992. **42**(4): p. 609-14.
27. Jolly, R.D. and D.N. Palmer, *The neuronal ceroid-lipofuscinoses (Batten disease): comparative aspects*. Neuropathology and Applied Neurobiology, 1995. **21**(1): p. 50-60.
28. Jolly, R.D. and D.M. West, *Blindness in South Hampshire sheep: a neuronal ceroidlipofuscinosis*. The New Zealand Veterinary Journal 1976. **24**(6): p. 123.
29. Cronin, G.M., et al., *Manifestation of neuronal ceroid lipofuscinosis in Australian Merino sheep: observations on altered behaviour and growth*. Applied Animal Behaviour Science, 2016. **175**: p. 32-40.
30. Tammen, I., et al., *Neuronal ceroid lipofuscinosis in Australian Merino sheep: a new animal model*. European Journal of Paediatric Neurology, 2001. **5 Suppl A**: p. 37-41.
31. Tammen, I., et al., *A missense mutation (c.184C>T) in ovine CLN6 causes neuronal ceroid lipofuscinosis in Merino sheep whereas affected South Hampshire sheep have reduced levels of CLN6 mRNA*. Biochimica et Biophysica Acta (BBA) - Molecular Basis of Disease, 2006. **1762**(10): p. 898-905.
32. Kay, G.W., et al., *Activation of non-neuronal cells within the prenatal developing brain of sheep with neuronal ceroid lipofuscinosis*. Brain Pathology, 2006. **16**(2): p. 110-6.
33. Zeinali, R., et al., *Brain Volume Estimation Enhancement by Morphological Image Processing Tools*. Journal of Biomedical Physics and Engineering, 2017. **7**(4): p. 379-388.
34. Oswald, M.J., et al., *Glial activation spreads from specific cerebral foci and precedes neurodegeneration in presymptomatic ovine neuronal ceroid lipofuscinosis (CLN6)*. Neurobiology of Disease, 2005. **20**(1): p. 49-63.
35. Mitchell, N.L., et al., *Characterisation of neuropathology in ovine CLN5 and CLN6 neuronal ceroid lipofuscinoses (Batten disease)* Developmental Neurobiology (submitted), 2022.
36. Russell, K.N., et al., *Electroretinography data from ovine models of CLN5 and CLN6 neuronal ceroid lipofuscinoses*. Data in Brief, 2021: p. 107188.
37. Mitchell, N.L., et al., *Longitudinal In Vivo Monitoring of the CNS Demonstrates the Efficacy of Gene Therapy in a Sheep Model of CLN5 Batten Disease*. Molecular Therapy, 2018. **26**(10): p. 2366-2378.
38. Morton, A.J. and D.S. Howland, *Large genetic animal models of Huntington's Disease*. Journal of Huntington's Disease, 2013. **2**(1): p. 3-19.
39. Yeo, J.D., et al., *The experimental contusion injury of the spinal cord in sheep*. Paraplegia, 1975. **12**(4): p. 279-98.
40. Yeo, J.D., S. Stabback, and B. McKenzie, *Central necrosis following contusion to the sheep's spinal cord*. Spinal Cord, 1977. **14**(4): p. 276-285.
41. Russell, K.N., et al., *Computed tomography provides enhanced techniques for longitudinal monitoring of progressive intracranial volume loss associated with regional neurodegeneration in ovine neuronal ceroid lipofuscinoses*. Brain and Behavior, 2018. **8**(9): p. e01096.
42. Bennett, M.L. and A.N. Viaene, *What are activated and reactive glia and what is their role in neurodegeneration?* Neurobiol Dis, 2021. **148**: p. 105172.
43. DiSabato, D.J., N. Quan, and J.P. Godbout, *Neuroinflammation: the devil is in the details*. Journal of Neurochemistry, 2016. **139**(Suppl 2): p. 136-153.

44. Chen, W.W., X. Zhang, and W.J. Huang, *Role of neuroinflammation in neurodegenerative diseases (Review)*. *Molecular Medicine Reports*, 2016. **13**(4): p. 3391-6.
45. Cooper, J.D., C. Russell, and H.M. Mitchison, *Progress towards understanding disease mechanisms in small vertebrate models of neuronal ceroid lipofuscinosis*. *Biochimica et Biophysica Acta (BBA) - Molecular Basis of Disease*, 2006. **1762**(10): p. 873-889.
46. Haltia, M., *The Neuronal Ceroid-Lipofuscinoses*. *Journal of Neuropathology & Experimental Neurology*, 2003. **62**(1): p. 1-13.
47. Gonçalves, G.A.R. and R.M.A. Paiva, *Gene therapy: advances, challenges and perspectives*. *Einstein (Sao Paulo)*, 2017. **15**(3): p. 369-375.
48. Wang, D., P.W.L. Tai, and G. Gao, *Adeno-associated virus vector as a platform for gene therapy delivery*. *Nature Reviews Drug Discovery*, 2019. **18**(5): p. 358-378.
49. Murray, S.J. and N.L. Mitchell, *The Translational Benefits of Sheep as Large Animal Models of Human Neurological Disorders*. *Frontiers in Veterinary Science*, 2022. **9**: p. 831838-831838.
50. Mitchell, N.L., et al., *Dose Escalation Studies of Intracerebroventricular CLN5 Gene Therapy in Sheep*. *Molecular Therapy (In preparation)*. 2022.
51. Murray, S.J., et al., *Intravitreal gene therapy protects against retinal dysfunction and degeneration in sheep with CLN5 Batten disease*. *Experimental Eye Research*, 2021. **207**: p. 108600.
52. Murray, S.J., et al., *Efficacy of Intracerebroventricular and Intravitreal CLN5 Gene Therapy in Sheep*. *Molecular Therapy (In preparation)*, 2022.
53. *Neurogene Announces FDA Clearance of IND for NGN-101 Gene Therapy to Treat CLN5 Batten Disease*. Available from: <https://www.neurogene.com/press-releases/neurogene-announces-fda-clearance-of-ind-for-ngn-101-gene-therapy-to-treat-cln5-batten-disease/>.
54. *Gene Therapy Study for Children With CLN5 Batten Disease (CLN5-200)*. Available from: <https://www.clinicaltrials.gov/ct2/show/study/NCT05228145?cond=cln5&draw=2&rank=1>.
55. Wilke, H.J., et al., *Anatomy of the sheep spine and its comparison to the human spine*. *The Anatomical Record*, 1997. **247**(4): p. 542-55.
56. Sheng, S.R., et al., *Anatomy of large animal spines and its comparison to the human spine: a systematic review*. *European Spine journal* 2010. **19**(1): p. 46-56.
57. Zeevalk, G.D., *13.02 - Fundamentals of the Structure and Function of the Nervous System*, in *Comprehensive Toxicology (Second Edition)*, C.A. McQueen, Editor. 2010, Elsevier: Oxford. p. 3-27.
58. Fung, P.C.W. and R.K.C. Kong, *New Insights on Stimulating the Lung Meridian Based on Modern Neurophysiology*. *Chinese Medicine*, 2018. **09**: p. 75-117.
59. Purves, D., et al., *The Internal Anatomy of the Spinal Cord*. 2001, Sinauer Associates (MA).
60. Marieb, E.N. and H. Katja, *Human anatomy & physiology*. 7th ed.. ed. Human Anatomy and Physiology, ed. K. Hoehn. 2007, San Francisco: Pearson Benjamin Cummings.
61. Cork, L.C., *Hereditary Canine Spinal Muscular Atrophy: An Animal Model of Motor Neuron Disease*. *Canadian Journal of Neurological Sciences*, 1991. **18**(S3): p. 432-434.
62. Katz, M.L., et al., *Cervical spinal cord and motor unit pathology in a canine model of SOD1-associated amyotrophic lateral sclerosis*. *Journal of the Neurological Sciences*, 2017. **378**: p. 193-203.
63. Uchida, A., et al., *Non-human primate model of amyotrophic lateral sclerosis with cytoplasmic mislocalization of TDP-43*. *Brain*, 2012. **135**(3): p. 833-846.
64. Xu, Y.F., et al., *Wild-type human TDP-43 expression causes TDP-43 phosphorylation, mitochondrial aggregation, motor deficits, and early mortality in transgenic mice*. *The Journal of Neuroscience*, 2010. **30**(32): p. 10851-9.
65. Wils, H., et al., *TDP-43 transgenic mice develop spastic paralysis and neuronal inclusions characteristic of ALS and frontotemporal lobar degeneration*. *Proceedings of the National Academy of Sciences of the United States of America*, 2010. **107**(8): p. 3858-63.
66. Shan, X., et al., *Altered distributions of Gemini of coiled bodies and mitochondria in motor neurons of TDP-43 transgenic mice*. *Proceedings of the National Academy of Sciences of the United States of America*, 2010. **107**(37): p. 16325-30.

67. Jalanko, A. and T. Braulke, *Neuronal ceroid lipofuscinoses*. Biochimica et Biophysica Acta (BBA) - Molecular Cell Research, 2009. **1793**(4): p. 697-709.
68. Nelvagal, H.R., et al., *Spinal manifestations of CLN1 disease start during the early postnatal period*. Neuropathology and Applied Neurobiology, 2021. **47**(2): p. 251-267.
69. Kielar, C., et al., *Successive neuron loss in the thalamus and cortex in a mouse model of infantile neuronal ceroid lipofuscinosis*. Neurobiology of Disease, 2007. **25**(1): p. 150-62.
70. Kwan, P., *Characterization of spinal cord lesions in CLN6 ovine model using microscopic analysis*. 2021: The University of Sydney.
71. Murray, S.J., et al., *Progressive MRI brain volume changes in ovine models of CLN5 and CLN6 neuronal ceroid lipofuscinosis*. Brain Communications, 2023. **5**(1).
72. Pontikis, C.C., et al., *Thalamocortical neuron loss and localized astrocytosis in the Cln3Deltaex7/8 knock-in mouse model of Batten disease*. Neurobiology of Disease, 2005. **20**(3): p. 823-36.
73. David, G., et al., *Extent of Cord Pathology in the Lumbosacral Enlargement in Non-Traumatic versus Traumatic Spinal Cord Injury*. Journal of Neurotrauma, 2022. **39**(9-10): p. 639-650.
74. Leplus, A., et al., *Chronic fornix deep brain stimulation in a transgenic Alzheimer's rat model reduces amyloid burden, inflammation, and neuronal loss*. Brain Structure and Function, 2019. **224**(1): p. 363-372.
75. Jiang, W., et al., *Dopamine inhibits pyroptosis and attenuates secondary damage after spinal cord injury in female mice*. Neuroscience Letters, 2022. **792**: p. 136935.
76. Schulz, A., et al., *NCL diseases - clinical perspectives*. Biochimica et Biophysica Acta (BBA) - Molecular Basis of Disease, 2013. **1832**(11): p. 1801-6.
77. Anderson, G.W., H.H. Goebel, and A. Simonati, *Human pathology in NCL*. Biochimica et Biophysica Acta (BBA) - Molecular Basis of Disease, 2013. **1832**(11): p. 1807-26.
78. Tyynelä, J., et al., *Hippocampal pathology in the human neuronal ceroid-lipofuscinoses: distinct patterns of storage deposition, neurodegeneration and glial activation*. Brain Pathology, 2004. **14**(4): p. 349-57.
79. Bible, E., et al., *Regional and cellular neuropathology in the palmitoyl protein thioesterase-1 null mutant mouse model of infantile neuronal ceroid lipofuscinosis*. Neurobiology of Disease, 2004. **16**(2): p. 346-59.
80. Macauley, S.L., et al., *Cerebellar pathology and motor deficits in the palmitoyl protein thioesterase 1-deficient mouse*. Experimental Neurology, 2009. **217**(1): p. 124-35.
81. Groh, J., et al., *Immune cells perturb axons and impair neuronal survival in a mouse model of infantile neuronal ceroid lipofuscinosis*. Brain, 2013. **136**(Pt 4): p. 1083-101.
82. Jiang, H., et al., *A comparison of spinal ligaments--differences between bipeds and quadrupeds*. Journal of Anatomy, 1995. **187 (Pt 1)**(Pt 1): p. 85-91.
83. Gittins, R. and P.J. Harrison, *Neuronal density, size and shape in the human anterior cingulate cortex: a comparison of Nissl and NeuN staining*. Brain Research Bulletin, 2004. **63**(2): p. 155-160.
84. Pamphlett, R., J. Kril, and T.M. Hng, *Motor neuron disease: a primary disorder of corticomotoneurons?* Muscle Nerve, 1995. **18**(3): p. 314-8.
85. Kerstetter, A.E. and R.H. Miller, *Isolation and culture of spinal cord astrocytes*. Methods in Molecular Biology, 2012. **814**: p. 93-104.
86. Lundgaard, I., et al., *White matter astrocytes in health and disease*. The Journal of Neuroscience, 2014. **276**: p. 161-73.
87. Emsley, J.G. and J.D. Macklis, *Astroglial heterogeneity closely reflects the neuronal-defined anatomy of the adult murine CNS*. Neuron Glia Biology, 2006. **2**(3): p. 175-86.
88. Al-karim, S., et al., *Histological and Immunohistochemical Effects of Neuroectodermal Cells Transplantation After Spinal Cord Injury in Rats*. International Journal of Morphology, 2019. **37**(1): p. 212-220.
89. Van Eycke, Y.R., et al., *Image processing in digital pathology: an opportunity to solve inter-batch variability of immunohistochemical staining*. Scientific Reports, 2017. **7**: p. 42964.

90. Craig, A.D., E.T. Zhang, and A. Blomqvist, *Association of spinothalamic lamina I neurons and their ascending axons with calbindin-immunoreactivity in monkey and human*. The Journal of Pain, 2002. **97**(1-2): p. 105-15.
91. Huang, Z.J., *Subcellular organization of GABAergic synapses: role of ankyrins and L1 cell adhesion molecules*. Nature Neuroscience, 2006. **9**(2): p. 163-6.
92. Ren, K. and M.A. Ruda, *A comparative study of the calcium-binding proteins calbindin-D28K, calretinin, calmodulin and parvalbumin in the rat spinal cord*. Brain Research Reviews, 1994. **19**(2): p. 163-79.
93. Anelli, R. and C.J. Heckman, *The calcium binding proteins calbindin, parvalbumin, and calretinin have specific patterns of expression in the gray matter of cat spinal cord*. Journal of Neurocytology, 2005. **34**(6): p. 369-85.
94. Brini, M., et al., *Neuronal calcium signaling: function and dysfunction*. Cellular and Molecular Life Sciences, 2014. **71**(15): p. 2787-814.
95. Siembab, V.C., et al., *Target selection of proprioceptive and motor axon synapses on neonatal V1-derived Ia inhibitory interneurons and Renshaw cells*. The Journal of Comparative Neurology, 2010. **518**(23): p. 4675-701.
96. Zhang, J.H., et al., *Ontological study of calbindin-D28k-like and parvalbumin-like immunoreactivities in rat spinal cord and dorsal root ganglia*. The Journal of Comparative Neurology, 1990. **302**(4): p. 715-28.
97. Merkulyeva, N., et al., *Distribution of 28 kDa Calbindin-Immunopositive Neurons in the Cat Spinal Cord*. Front Neuroanatomy, 2015. **9**: p. 166.
98. Chen, S., et al., *A Comparative Study of Three Interneuron Types in the Rat Spinal Cord*. PLOS One, 2016. **11**(9): p. e0162969.
99. Floyd, T.L., Y. Dai, and D.R. Ladle, *Characterization of calbindin D28k expressing interneurons in the ventral horn of the mouse spinal cord*. Developmental Dynamics, 2018. **247**(1): p. 185-193.
100. Petitjean, H., et al., *Recruitment of Spinoparabrachial Neurons by Dorsal Horn Calretinin Neurons*. Cell Reports, 2019. **28**(6): p. 1429-1438.e4.
101. Dowlati, E., *Spinal cord anatomy, pain, and spinal cord stimulation mechanisms*. Seminars in Spine Surgery, 2017. **29**(3): p. 136-146.
102. Chang, I.Y., et al., *Calbindin D-28k, parvalbumin and calcitonin gene-related peptide immunoreactivity in the canine spinal cord*. Anatomia, Histologia, Embryologia, 2008. **37**(6): p. 446-51.
103. Chakrabarty, S., B. Shulman, and J.H. Martin, *Activity-dependent codevelopment of the corticospinal system and target interneurons in the cervical spinal cord*. Journal of Neurocytology, 2009. **29**(27): p. 8816-27.
104. Zhang, M.D., et al., *Comparative anatomical distribution of neuronal calcium-binding protein (NECAB) 1 and -2 in rodent and human spinal cord*. Brain Structure and Function, 2016. **221**(7): p. 3803-23.
105. Murray, S.J. and N.L. Mitchell, *Natural history of retinal degeneration in ovine models of CLN5 and CLN6 neuronal ceroid lipofuscinoses*. Scientific Reports, 2022. **12**(1): p. 3670.
106. Rodríguez-Barrera, R., et al., *Neurogenesis after Spinal Cord Injury: State of the Art*. Cells, 2021. **10**(6).
107. Havelikova, K., B. Smejkalova, and P. Jendelova, *Neurogenesis as a Tool for Spinal Cord Injury*. International Journal of Molecular Sciences, 2022. **23**(7).
108. Rusanescu, G., *Adult spinal cord neurogenesis: A regulator of nociception*. Neurogenesis, 2016. **3**(1): p. e1256853.
109. Seehafer, S.S. and D.A. Pearce, *You say lipofuscin, we say ceroid: defining autofluorescent storage material*. Neurobiology of Aging, 2006. **27**(4): p. 576-88.
110. Ostergaard, J.R., H.R. Nelvagal, and J.D. Cooper, *Top-down and bottom-up propagation of disease in the neuronal ceroid lipofuscinoses*. Frontiers in Neurology, 2022. **13**: p. 1061363-1061363.